

Bifurcation analysis and control study of improved full-speed differential model in connected vehicle environment

Wen-Huan Ai(艾文欢), Zheng-Qing Lei(雷正清), Dan-Yang Li(李丹洋), Dong-Liang Fang(方栋梁), and Da-Wei Liu(刘大为)

Citation: Chin. Phys. B, 2024, 33 (**7**): 070503. DOI: 10.1088/1674-1056/ad3b80
Journal homepage: http://cpb.iphy.ac.cn; http://iopscience.iop.org/cpb

What follows is a list of articles you may be interested in

Bifurcation analysis of visual angle model with anticipated time and stabilizing driving behavior

Xueyi Guan(管学义), Rongjun Cheng(程荣军), and Hongxia Ge(葛红霞)
Chin. Phys. B, 2022, 31 (**7**): 070507. DOI: 10.1088/1674-1056/ac5606

Extremely hidden multi-stability in a class of two-dimensional maps with a cosine memristor

Li-Ping Zhang(张丽萍), Yang Liu(刘洋), Zhou-Chao Wei(魏周超), Hai-Bo Jiang(姜海波), Wei-Peng Lyu(吕伟鹏), and Qin-Sheng Bi(毕勤胜)
Chin. Phys. B, 2022, 31 (**10**): 100503. DOI: 10.1088/1674-1056/ac7294

Stabilization strategy of a car-following model with multiple time delays of the drivers

Weilin Ren(任卫林), Rongjun Cheng(程荣军), and Hongxia Ge(葛红霞)
Chin. Phys. B, 2021, 30 (**12**): 120506. DOI: 10.1088/1674-1056/abfcc9

A novel class of two-dimensional chaotic maps with infinitely many coexisting attractors

Li-Ping Zhang(张丽萍), Yang Liu(刘洋), Zhou-Chao Wei(魏周超), Hai-Bo Jiang(姜海波), Qin-Sheng Bi(毕勤胜)
Chin. Phys. B, 2020, 29 (**6**): 060501. DOI: 10.1088/1674-1056/ab8626

Effect of magnetic flow and external forcing current on mixed bursting in the pre-Bötzinger complex

Dou-Dou Guo(郭豆豆), Zhuo-Sheng Lü(吕卓生)
Chin. Phys. B, 2019, 28 (**11**): 110501. DOI: 10.1088/1674-1056/ab43b9

Bifurcation analysis and control study of improved full-speed differential model in connected vehicle environment

Wen-Huan Ai(艾文欢)[1,†], Zheng-Qing Lei(雷正清)[1], Dan-Yang Li(李丹洋)[1], Dong-Liang Fang(方栋梁)[1], and Da-Wei Liu(刘大为)[2]

[1] *College of Computer Science and Engineering, Northwest Normal University, Lanzhou* 730070, *China*
[2] *College of Electrical Engineering, Lanzhou Institute of Technology, Lanzhou* 730050, *China*

(Received 17 November 2023; revised manuscript received 14 March 2024; accepted manuscript online 7 April 2024)

In recent years, the traffic congestion problem has become more and more serious, and the research on traffic system control has become a new hot spot. Studying the bifurcation characteristics of traffic flow systems and designing control schemes for unstable pivots can alleviate the traffic congestion problem from a new perspective. In this work, the full-speed differential model considering the vehicle network environment is improved in order to adjust the traffic flow from the perspective of bifurcation control, the existence conditions of Hopf bifurcation and saddle-node bifurcation in the model are proved theoretically, and the stability mutation point for the stability of the transportation system is found. For the unstable bifurcation point, a nonlinear system feedback controller is designed by using Chebyshev polynomial approximation and stochastic feedback control method. The advancement, postponement, and elimination of Hopf bifurcation are achieved without changing the system equilibrium point, and the mutation behavior of the transportation system is controlled so as to alleviate the traffic congestion. The changes in the stability of complex traffic systems are explained through the bifurcation analysis, which can better capture the characteristics of the traffic flow. By adjusting the control parameters in the feedback controllers, the influence of the boundary conditions on the stability of the traffic system is adequately described, and the effects of the unstable focuses and saddle points on the system are suppressed to slow down the traffic flow. In addition, the unstable bifurcation points can be eliminated and the Hopf bifurcation can be controlled to advance, delay, and disappear, so as to realize the control of the stability behavior of the traffic system, which can help to alleviate the traffic congestion and describe the actual traffic phenomena as well.

Keywords: bifurcation analysis, vehicle queuing, bifurcation control, Hopf bifurcation

PACS: 05.45.–a, 47.52.+j, 45.70.Vn **DOI:** 10.1088/1674-1056/ad3b80

1. Introduction

In the contemporary era of rapid economic development, economic loss, environmental pollution, and energy consumption caused by traffic congestion have become important issues affecting the national economy and people's livelihood. There have been fewer mixed traffic behaviors such as pedestrians and lane changes on highways, various traffic phenomena such as phantom traffic jams, smooth traffic flow, vehicles walking and stopping, and synchronous flow often appear alternately, thus leading to further aggravation of traffic congestion. However, it is difficult to find out the mechanism that triggers off these changes, which creates new requirements for highway traffic congestion mitigation and control. With the rapid development of smart city construction and connected vehicles, traffic system control research has become a new hot spot.

Traffic flow models are the main tools to carry out the theoretical research on traffic flow, and they can reveal the essential properties of various traffic flow phenomena, reproduce and explain the formation process and evolution law of complex traffic flow. The models of traffic behavior are divided into two types: microscopic model and macro model. The microscopic model mainly studies the state of rear vehicles following the front vehicle in a single lane in a queue. In the process of simulating the movement of a single vehicle on an urban road, a variety of factors have been considered such as vehicle performance and inter-vehicle interactions,[1–3] the influence of driver behavior and attributes,[4,5] the influence of pavement quality and road conditions,[6–8] the influence of the information environment and weather conditions,[9,10] *etc*. The models have been established, and simulations and analyses have been carried out. Most of the studies on highway traffic flow focused on macro traffic flow modeling and analysis. The traffic flow were regarded as a continuous fluid medium and a large number of gas models and fluid dynamics models were used[11–13] to describe the traffic phenomenon, and a large number of macro traffic flow models have been proposed. This class of model mainly involved the continuity equation and the velocity–density relationship of traffic flow, which can better describe the collective behavior of traffic flow. Currently, the bifurcation phenomenon of traffic flow mainly has been investigated based on the follower model. Zhang *et al*. conducted a Hopf bifurcation analysis based on a newly proposed follower model considering time-lag speed difference, and examined the effect of time-lag

[†]Corresponding author. E-mail: wenhuan618@163.com

© 2024 Chinese Physical Society and IOP Publishing Ltd

speed on traffic flow through theoretical analysis and numerical simulation.[14] Ngoduy and Li investigated the bifurcation phenomenon in a class of Hopf bifurcation phenomenon in time-lagged follow-through model and constructed a generalized bifurcation structure for follow-through models considering multiple time delays.[15] In the same year, Jin and Meng studied the dynamics of an optimal speed model with differential speed delay feedback control, selecting the time delays and feedback gains from the corresponding stable intervals, and the proposed control strategy can effectively suppress traffic congestion and significantly improve the stability of the traffic flow.[16] Petersik *et al*. conducted a bifurcation analysis of a variety of artificial neural network-based automobile heeling models for bifurcation analysis and found that subcritical Hopf bifurcation can make vehicle flow change stability.[17]

However, there are few researches on analyzing the traffic flow bifurcation phenomenon based on macro traffic flow models, and some researches only partially address this aspect. Li used the discrete form of Payne's model to show that the appearance of bifurcation points can lead to the transformation of the traffic flow pattern from free flow to synchronous flow, and that chaotic phenomena can lead to the emergence of traffic congestion.[18] Ren *et al*. investigated the Hopf bifurcation phenomenon in a heterogeneous traffic flow model incorporating the driver's psychological headway differences and the self-stabilization effect on the psychological headway, which in turn leads to the analysis of Hopf bifurcation in a heterogeneous traffic flow model considering the variation of the electronic throttle angle with memory, which was set as the starting point of a heterogeneous continuous traffic flow to analyze the heterogeneous evolution of bifurcation behavior in traffic flow.[20,21] Lyu *et al*. performed an analysis of Hopf bifurcation based on a newly proposed macro traffic flow model, and their study showed that the occurrence of Hopf bifurcation has a significant influence on the stability of the traffic flow, resulting in equal-amplitude oscillations in the density wave of the traffic flow.[22] The bifurcation analysis method is not widely used in traffic flow theory, especially the use of bifurcation theory to analyze, predict, and control the actual traffic phenomenon has not been well solved.

The objective of bifurcation control is to design a feedback controller to change the bifurcation characteristics of the system in order to obtain the desired dynamic behavior. Typical bifurcation controls include the delaying of the inherent bifurcation behavior of the original system, the changing of the parameter values or design parameters corresponding to the system at the bifurcation point to make a new bifurcation, the changing of the location of the equilibrium point, the changing of the topology of the original nonlinear system as well as the type of bifurcation, and the changing of the diversity and amplitude of the original limit loop. Currently, the main methods of controlling bifurcation are to control the linear feedback, nonlinear feedback,[23–25] and delayed feedback,[26,27] approximation methods, normative type methods, and others.[28,29] The bifurcation control method is to effectively control the bifurcation dynamics behavior of the system by adjusting the control parameters and feedback gain of the controller and extending the feedback delay, exploring the relationship between the time delay and bifurcation of the system, introducing the delayed feedback controller into the proposed system, and changing the effect of the change of the feedback gain on the bifurcation, so as to achieve asymptotically stabilizing control of the unstable system.[30,31] In many studies in China, it is to set a nonlinear controller to be the system for Hopf bifurcation and stability control. The corresponding relations among the bifurcation parameters, stability parameters and control parameters are obtained through analyses, and then the control parameters of the controller are adjusted to achieve the behaviors such as Hopf bifurcation delay and bifurcation solution stability range change of the system.[32] Bifurcation analysis, as an emerging nonlinear analysis method, can finely dissect the subtle dynamics that can occur in a nonlinear system with the change of its parameters, which is potentially advantageous for controlling the behavior of stability mutations in transportation systems.

However, there is less literature on the use of bifurcation analysis methods for studying the traffic control. In the research on bifurcation control based on transportation systems, Cheng *et al*. conducted a two-parameter bifurcation analysis based on a railroad wheelset model, and it was pointed out that the supercritical bifurcation and subcritical bifurcation, which divide the bifurcation curves through generalized Hopf points, play a key role in determining the occurrence of wheel flange lifting and derailment of high-speed railroad vehicles.[33] In the same year, Wang *et al*. investigated the bifurcation phenomenon in a class of non-uniform traffic flow models containing multiple vehicles, and in order to describe the interactions between different types of vehicles, bifurcation analysis was applied to study the laws of the magnitude of the inter-vehicle spacing in the traffic system.[34] Kamath *et al*. investigated the effect of delayed feedback on the dynamics of a classical car following model (CCFM) and demonstrated that the transition of the traffic flow from a locally steady state to an unstable state occurs through Hopf bifurcation, which leads to limit cycles in the dynamics of the system, providing phenomenological insights into the effect of delayed feedback control on the emergence and evolution of traffic congestion.[35] Newell carried out a bifurcation analysis based on a microscopic traffic flow model and obtained the existence condition of Hopf bifurcation for their model.[36] In the same year, Ren *et al*. proposed an OVM-based traffic flow model, based on which bifurcation analysis was carried

out, and based on which a feedback control study was carried out by considering the driver's expectation and response delay, and it was shown that the Hopf bifurcation phenomenon caused by small disturbances can be suppressed by a feedback controller.[37] The innovation of this work lies in the design of a nonlinear stochastic feedback controller to study the bifurcation phenomenon and control process in a nonlinear transportation system, in order to delay or eliminate the occurrence of bifurcation and change the behavior of bifurcation types; by controlling the amplitude of the limit ring, etc., the stability of the transportation system can be improved, providing a theoretical basis for preventing and alleviating traffic congestion. For the control of nonlinear stochastic dynamical system, it is mainly realized by studying the change of bifurcation points in the system model and the change of system stability after adding a nonlinear feedback controller. That is, the stochastic problem of the system is transformed into a bifurcation-controlling problem for its equivalent deterministic system by means of Chebyshev polynomial approximation, so as to design the feedback controller to realize the delay and change of the Hopf bifurcation of the system. The delay and disappearance of the bifurcation points are achieved by adjusting the values of the control parameters of the controlled system model to achieve the effect of controlling the transportation system.

The rest of this paper is arranged as follows. In Section 2, we introduce the background of the problem and propose our new model based on the traditional full velocity difference model. In Section 3, the linear stability condition of the model is derived. In Section 4, the model is analyzed nonlinearly to obtain a linear system with stochastic control model. In Section 5, the existence conditions of Hopf bifurcation and saddle-node bifurcation of the model and the setup procedure of feedback controller for Hopf bifurcation are derived. In the experimental part of Section 6, the phase, density spatio-temporal and bifurcation diagrams for different traveling wave speeds and feedback controllers are plotted by characterizing the critical points of the bifurcation points, which provide a strong support and validation for the theoretical part of this paper. Finally, Section 7 is devoted to the summation of this study, points out the shortcomings of the work, and looks forward to the next step.

2. Improved full-speed differential model in connected vehicle environment

In order to describe the dynamic behavior of high-density vehicles on a single lane, Newell established one of the most famous traffic models, which is called optimal velocity model (OVM).[36] The OVM can successfully describe some real traffic phenomena, such as stop and go, traffic jam, and so on. However, compared with the actual data, the acceleration of OVM is too large and its deceleration is unrealistic. Therefore, Ren *et al*. proposed the full velocity difference model (FVD),[37] which replaced the density gradient term with velocity gradient. The FVD model is described as follows:

$$\frac{\mathrm{d}v_n(t)}{\mathrm{d}t} = a[V(\Delta x_n(t)) - v_n(t)] + \lambda \Delta v_n(t), \tag{1}$$

where a and λ are two reaction coefficients, $v_n(t)$ represents the speed of vehicle n at time t, and $V(\Delta x_n(t))$ denotes the optimal speed function.

In the actual traffic it is often observed that the distance between the vehicle and the vehicle in front is much greater than the safety distance, but the driver still maintains a similar speed to the surrounding vehicles and does not accelerate to shorten the distance from the vehicle in front. This will result in most sections of urban roads being idle, which is unconducive to smooth traffic. In order to verify this phenomenon, we take the traffic video data collected from the 7.6-meter-high overpass of Lanzhou Beibinhe Road at 7:15 a.m. in the morning rush hour as an example. The spacing between vehicles is calculated by measuring the spacing between the white marking lines of the actual road lanes. Urban expressways usually have dense, uniform steady-state traffic flow characteristics. This traffic flow has certain fluid properties such as mobility, fluctuation, surge, compression, and diffusion, which makes the macro traffic flow model a suitable descriptive tool.[38] To verify the traffic flow characteristics of the morning peak, we plot an actual driving road map, inter-vehicle distance versus time graph, and speed versus time graph are obtained as shown in Fig. 1.

From Fig. 1(a), we can see that for cars labeled 1, 2, 3, 4, 5, and 6 in the video, the spacing between car 1 and car 2 is 7 m, the spacing between car 2 and car 3 is 6.5 m, the spacing between car 5 and car 6 is 8 m, but the spacing between car 4 and car 5 is 20 m, which is a great waste of road, and is unconducive to improving traffic flow. From Fig. 1(b), we can see that the spacing between car 1 and car 5 in the video is between 7 m and 8.5 m, which greatly increases the road utilization rate and helps to reduce traffic congestion. From Fig. 1(c), we can see that the inter-vehicle distances between car 2, car 3, and car 4 do not fluctuate much over time, and each vehicle floats above and below its respective baseline. In this traffic flow state, the relative position between vehicles changes less, and the distance between vehicles remains relatively stable. And the speed over time fluctuation graph is also consistent with this situation, when the driver travelling speed is relatively consistent, the inter-vehicle distance will remain relatively stable. This state is in line with the traffic flow characteristics of dense and uniform steady state, therefore, this video can be used to carry out bifurcation analysis and other researches on the macro traffic flow model.

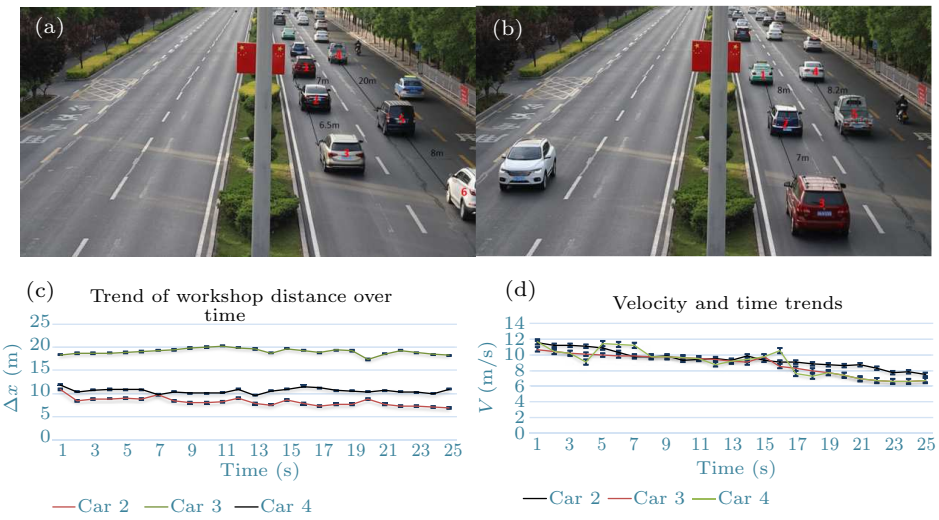


Fig. 1. (a)–(b) Traffic flow, (c) inter-vehicle distance versus time, and (d) speed versus time.

For a real transportation system, vehicles traveling on the road are easily affected by various random interference factors. Especially with the development of intelligent transportation, the drawbacks of the FVD model are becoming more and more prominent, and it is unable to accurately describe the real traffic situation in the car network environment. Therefore, this paper focuses on analyzing the characteristics of real-time detection of road conditions and timely detection of driver fatigue in vehicle networking environment, and considers the influence of vehicle–vehicle communication to construct a macro traffic flow model more suitable for vehicle networking environment.

Based on the consideration of vehicle–vehicle communication, it is found that the existing literature has less consideration of the influence on traffic flow in the context of connected vehicles. In the context of connected vehicles, real-time communication between vehicles can be achieved through the network as shown in Fig. 2. By determining the distance between the vehicle and the vehicle in front, it is recommended that the driver should accelerate or decelerate to maintain an appropriate distance from the vehicle in front. This is beneficial for improving road utilization and reducing traffic congestion.

By collecting and analyzing communication data between vehicles, researchers can more accurately understand the dynamics of traffic flows. With the support of vehicle-to-vehicle communication, the bifurcation analysis can more accurately predict the bifurcation points of the traffic flow, understand the congestion points, and bottleneck areas of the traffic flow, and then optimize the traffic organization. The bifurcation analysis of macro traffic flow model can be combined with intelligent traffic control system to achieve real-time traffic control. For example, by the real-time monitoring of the traffic flow status, the timing of traffic signals can be adjusted to optimize the organization and scheduling of the traffic flow, reducing the likelihood of traffic congestion and accidents. Bifurcation analysis through the macro traffic flow model can also be used to assess the effectiveness of traffic policies. For example, after the implementation of a new traffic policy, bifurcation analysis can be used to simulate the changes in traffic flow, in order to evaluate the effectiveness and feasibility of the policy.

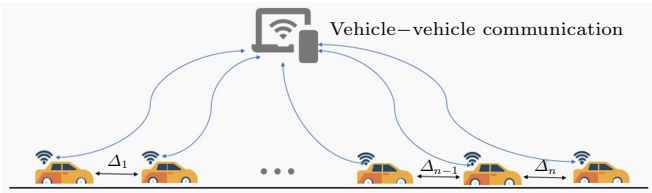


Fig. 2. Schematic diagram of vehicle-to-vehicle communication network.

In order to better describe the changing state of traffic flow in the environment of connected vehicles, we discuss the classification of the distance between front vehicle and rear vehicle based on the recognition range of the adaptive cruise control system, making the new model closer to the real traffic flow state of connected vehicles.

(i) The current rear inter-vehicle distance is greater than the range recognized by the adaptive cruise system. ξ_n is introduced to represent the disturbance of the adaptive cruise system,[38] and it is expressed as

$$\xi_n = \begin{cases} 0, & \Delta > x_0, \\ \tanh\left(\dfrac{\Delta}{x_0} - \varepsilon\right)\Delta v_n(t), & \Delta \le x_0, \end{cases} \tag{2}$$

where Δ represents the distance between vehicles, x_0 the distance recognized by the adaptive cruise system, and ε the distance ratio correction parameter. When the current rear vehicles are far away, the inter-vehicle distance Δ is greater than the recognition range x_0 of the adaptive cruise system, that is, $\Delta > x_0$. At this time, the adaptive cruise system cannot recognize the front and rear vehicles, and the vehicle running state is not disturbed by the adaptive cruise system. Disturbance term $\xi_n(t) = 0$, the new model is the same as FVD model. The new

model is as follows:

$$\frac{\mathrm{d}v_n(t)}{\mathrm{d}t} = a[V(\Delta x_n(t)) - v_n(t)] + \lambda \Delta v_n(t). \tag{3}$$

(ii) The current rear inter-vehicle distance is within the range recognized by the adaptive cruise system.

Let $\theta_n(t)$ represent the influence state of the acceleration and deceleration of the front vehicle on the rear vehicle under the influence of the internet of vehicles, and a_{n+1} denote the acceleration of the vehicle in front. The expression of $\theta_n(t)$ is as follows:

$$\theta_n(t) = \begin{cases} -1, & a_{n+1} \le 0, \\ 1, & a_{n+1} > 0. \end{cases} \tag{4}$$

When the distance between the front and rear vehicles is within the recognizable range, the inter-vehicle distance Δ is within the recognizable range x_0 of the adaptive cruise system. At this time, the adaptive cruise system can recognize the front and rear vehicles. At this time $\Delta < x_0$, the disturbance item $\xi_n = \tanh(\Delta/x_0 - 0.8)\Delta v_n(t)$, and the vehicle running state will be disturbed by the adaptive cruise system. That is, when the front vehicle decelerates, the following vehicle will also decelerate, and when the front vehicle accelerates, the following vehicle will also accelerate. The new model is as follows:

$$\frac{\mathrm{d}v_n(t)}{\mathrm{d}t} = a[V(\Delta x_n(t)) - v_n(t)] + \lambda \Delta v_n(t) + \theta_n(t)\xi_n(t). \tag{5}$$

(iii) Only for one-way lanes and no overtaking.

The model will be aimed at one-way lanes without overtaking, where one-way lanes refer to two lanes that allow only one direction of travel. Because the micro car following model simulates the motion of vehicles following each other on a one-way lane without overtaking.

Based on the above three assumptions, an improved full speed difference model is proposed based on FVD model. The model is described as follows:

$$\frac{\mathrm{d}v_n(t)}{\mathrm{d}t} = a[V(\Delta x_n(t)) - v_n(t)] + \lambda \Delta v_n(t) + \theta_n(t)\xi_n(t), \tag{6}$$

where a and λ are two reaction coefficients, $v_n(t)$ represents the speed of vehicle n at time t, and $V(\Delta x_n(t))$ denotes the optimal speed function.

In Eq. (6), $\theta_n(t)$ represents the influential state of the acceleration and deceleration of the front vehicle on the rear vehicle under the influence of the internet of vehicles. The expression of $\theta_n(t)$ is as follows:

$$\theta_n(t) = \begin{cases} -1, & a_{n+1} \le 0, \\ 1, & a_{n+1} > 0. \end{cases} \tag{7}$$

In Eq. (6), ξ_n is introduced to represent the disturbance of the adaptive cruise system, and the expression of ξ_n is as follows:

$$\xi_n = \begin{cases} 0, & \Delta > x_0, \\ \tanh\left(\dfrac{\Delta}{x_0} - \varepsilon\right)\Delta v_n(t), & \Delta \le x_0, \end{cases} \tag{8}$$

where Δ represents the distance between vehicles and x_0 denotes the distance recognized by the adaptive cruise system.

The above micro variables are converted into macro variables and micro equations into continuous models as indicated below:

$$\begin{aligned} &v_n(t) \to v(x,t), \quad v_{n+1}(t) \to v_{n+1}(x+\Delta, t), \\ &V(\Delta x_n(t)) \to V_{\mathrm{e}}(\rho), \quad V'(\Delta x_n(t)) \to \bar{V}'(h), \end{aligned} \tag{9}$$

where $v(x,t)$ and $\rho(x,t)$ represent the macro velocity and macro density, where $h = 1/\rho$ and $V_{\mathrm{e}}(\rho)$ denote the equilibrium velocity, $\bar{V}'(h) = -\rho^2 V_{\mathrm{e}}'(\rho)$ and $\lambda = 1/\eta$ ignore the higher-order terms, and expand $\Delta v_n(t)$ into a Taylor series: $\Delta v_n(t) = v(x+\Delta, t) - v(x,t) = v_x \Delta + (1/2)v_{xx}\Delta^2$. Bring it into the micro model yields

$$\begin{cases} \dfrac{\partial \rho}{\partial t} + \dfrac{\partial(\rho v)}{\partial x} = 0, \\ \dfrac{\partial v}{\partial t} + (v - \lambda\Delta - M\Delta)\dfrac{\partial v}{\partial x} = \dfrac{V_{\mathrm{e}}(\rho) - v}{T} + \dfrac{1}{2}(\lambda + M)\Delta^2 v_{xx}, \end{cases} \tag{10}$$

where $M = \tanh(\frac{\Delta}{x_0} - \varepsilon)$.

The core parameters of the model and their denotation are summarized in Table 1.

Table 1. Core parameters of the model.

Parameter	Symbol
Driver's sensitivity	a
Weight coefficient	λ
Acceleration of the vehicle in front	a_{n+1}
Radiation effect of the preceding vehicle on the present vehicle	$\theta_n(t)$
Workshop distance	Δ
Recognizable range of the adaptive cruise system	x_0
Interference items from the preceding vehicle to the current vehicle	ξ_n

3. Linear analysis

Based on the full speed difference model, this section proposes a model considering the influence of vehicle networking environment. The model is described as follows:

$$\begin{cases} \dfrac{\partial \rho}{\partial t} + \dfrac{\partial(\rho v)}{\partial x} = 0, \\ \dfrac{\partial v}{\partial t} + (v - \lambda\Delta - M\Delta)\dfrac{\partial v}{\partial x} = \dfrac{V_{\mathrm{e}}(\rho) - v}{T} + \dfrac{1}{2}(\lambda + M)\Delta^2 v_{xx}. \end{cases} \tag{11}$$

Firstly, the linear stability analysis method is used to study the stability conditions of the model shock wave.

It is assumed that the initial traffic flow is a stable traffic flow with small disturbance. As done in Ref. [38], the traffic flow is decomposed into

$$\begin{aligned} \rho(x,t) &= \rho_0 + \textstyle\sum_k \hat{\rho}_k \exp(\mathrm{i}kx + \sigma_k t), \\ v(x,t) &= v_0 + \textstyle\sum_k \hat{v}_k \exp(\mathrm{i}kx + \sigma_k t), \end{aligned} \tag{12}$$

where $(\bar{\rho}(x), v(\bar{x}))$ is stable shock wave solution of model (11). Equation (12) is replaced with Eq. (11) and the resulting equation is linearized, the higher-order terms of disturbance $\hat{\rho}_k$ and $\hat{v}_k$ are ignored, and the following equation is obtained:

$$\begin{cases} (\sigma_k + \mathrm{i}kv_0)\hat{\rho}_k + \mathrm{i}k\rho_0\hat{v}_k = 0, \\ \dfrac{V_e'(\rho_0)}{T}\hat{\rho}_k - \left[\dfrac{1}{2}(\lambda+M)\Delta^2k^2 + \sigma_k + \dfrac{1}{T} + (v_0 - \lambda\Delta - M\Delta)\mathrm{i}k\right]\hat{v}_k = 0. \end{cases} \tag{13}$$

Equation (13) is rewritten in the matrix form as follows:

$$\begin{bmatrix} \sigma_k + \mathrm{i}kv_0 & \mathrm{i}k\rho_0 \\ \dfrac{V_e'(\bar{\rho})}{T} & \dfrac{1}{2}(\lambda+M)\Delta^2k^2 + \sigma_k + \dfrac{1}{T} + (v_0 - \lambda\Delta - M\Delta)\mathrm{i}k \end{bmatrix} \begin{bmatrix} \hat{\rho}_k \\ \hat{v}_k \end{bmatrix} = 0. \tag{14}$$

The equation has a nontrivial solution only when the determinant of its coefficient matrix is zero, so the following quadratic equation is obtained:

$$\begin{aligned} &(\sigma_k + \mathrm{i}kv_0)^2 + \frac{\mathrm{i}k\rho_0 V_e'(\rho_0)}{T} \\ &+ \left[\frac{1}{T} + \frac{1}{2}(\lambda+M)\Delta^2k^2 - (\lambda+M)\Delta\,\mathrm{i}k\right](\mathrm{i}kv_0 + \sigma_k) = 0. \end{aligned} \tag{15}$$

Consider the long wave expansion, let $\mathrm{i}k \approx 0$, $\sigma_k = \sigma_1(\mathrm{i}k) + \sigma_2(\mathrm{i}k)^2 + \cdots$, substitute it into Eq. (15), and separate the real part and imaginary part. Thus, the following equation is obtained:

$$\left(\frac{1}{T} + 2\bar{v}_x\right)(\sigma_1 + \bar{v}) - (\lambda+M)\bar{\rho}_x + \frac{\bar{\rho}V_e'(\bar{\rho})}{T} = 0, \tag{16}$$

$$\begin{aligned} &(\sigma_1 + \bar{v})^2 + \left(\frac{1}{T} + 2\bar{v}_x\right)\sigma_2 - (\sigma_1 + \bar{v})(\lambda+M) \\ &+ \left(\mu_0 + \frac{1}{2}(\lambda+M)\right)\bar{v}_x = 0, \end{aligned} \tag{17}$$

evidently

$$\sigma_1 = -\bar{v} + \frac{T(\lambda+M)\bar{v}_x - \bar{\rho}V_e'(\bar{\rho})}{1+2T\bar{v}_x}, \tag{18}$$

$$\begin{aligned} \sigma_2 = &-T\frac{(T(\lambda+M)\bar{v}_x - \bar{\rho}V_e'(\bar{\rho}))^2}{(1+2T\bar{v}_x)3} \\ &+ T(\lambda+M)\frac{T(\lambda+M)\bar{v}_x - \bar{\rho}V_e'(\bar{\rho})}{1+2T\bar{v}_x} \\ &+ \frac{T\bar{v}_x(\mu_0 + \frac{1}{2}(\lambda+M))}{1+2T\bar{v}_x}. \end{aligned} \tag{19}$$

The stability condition of model (11) depends on the real part of σ_k. In fact, when $\sigma_2 \geq 0$, model (12) is stable. It can be seen from Eq. (19) that the viscosity coefficient μ gradually increases and its stability will gradually lose in the stable state.

In fact, the stability condition of uniform traffic flow (ρ_0, v_0) can also be considered. Through the above discussion, the following conclusions are drawn: for uniform traffic flow (ρ_0, v_0), there are

$$\sigma_1 = -[v_0 + \rho_0 V_e'(\rho_0)], \tag{20}$$

$$\sigma_2 = -\frac{1}{T}\rho_0 V_e'(\rho_0)[(\lambda+M) + \rho_0 V_e'(\rho_0)]. \tag{21}$$

When $\sigma_2 \geq 0$, the uniform traffic flow (ρ_0, v_0) is stable, that is, the linear stability condition of model (11) is

$$(\lambda+M) + \rho_0 V_e'(\rho_0) \geq 0,$$

$$\mathrm{Im}(\theta_k) = -k\left[v_0 + \rho_0 V'(\rho_0)\right] + O\left(k^3\right). \tag{22}$$

The propagation speed of small disturbances can be derived from Eq. (22) and expressed as $v_0 + \rho_0 V'(\rho_0)$.

4. Nonlinear analysis

The type of equilibrium point and its stability of the system can reflect the situation of traffic flow. By using the traveling wave substitution of the system, the equilibrium point is studied, the phase plane near the equilibrium point is drawn, and the equilibrium point is compared to better reflect the stability changes near different equilibrium points. According to a new traffic flow model based on a high-order continuum, the model is composed of the following two equations: a local conservation equation of vehicle number $\frac{\partial\rho}{\partial t} + \frac{\partial(\rho v)}{\partial x} = 0$ and an equation of motion:

$$\begin{aligned} &\frac{\partial v}{\partial t} + (v - \lambda\Delta - M\Delta)\frac{\partial v}{\partial x} \\ &= \frac{V_e(\rho) - v}{T} + \frac{1}{2}(\lambda+M)\Delta^2 v_{xx}. \end{aligned} \tag{23}$$

The model uses periodic boundary conditions. In fact, the traffic phenomenon generated by bifurcation points is more obvious in the open loop section than in the closed loop section. Therefore, this paper is on the assumption that the main section is under an open boundary condition, that is,

$$\begin{cases} \rho(1,t) = \rho(2,t)\cdots\rho(L,t) = \rho(L-1,t), \\ v(1,t) = v(2,t)\cdots v(L,t) = v(L-1,t). \end{cases} \tag{24}$$

Suppose that the model has traveling wave solutions $\rho(z)$ and $v(z)$, where $z = x - ct$ is the traveling wave velocity $c < 0$. By using the above results and substituting them into equation $\partial\rho/\partial t + \partial(\rho v)/\partial x = 0$ and Eq. (24), the following results can be obtained: $-c\rho_z + q_z = 0$, and

$$\begin{aligned} &-c\frac{\partial v}{\partial z} + (v - \lambda\Delta - M\Delta)\frac{\partial v}{\partial z} \\ &= \frac{1}{T}(V_e(\rho) - v) + \frac{1}{2}(\lambda+M)\Delta^2\frac{\partial^2 v}{\partial z^2}. \end{aligned} \tag{25}$$

From formula $-c\rho_z + q_z = 0$, it can be inferred that $q_z = c\rho_z$. To obtain the derivative of z at both ends of the equation $\rho v = q$, at the same time there should be $q_z = \rho v_z + v\rho_z$. From formula $q_z = c\rho_z$ and formula $q_z = \rho v_z + v\rho_z$, then $v_z = c\rho_z/\rho -$

$q\rho_z/\rho^2$ and $v_{zz} = [(c\rho - q)/\rho^2]\rho_{zz}$. Meanwhile, integrating equation with respect to z yields $-c\rho + q = \text{const} = q_*$. At the same time $q = q_* + c\rho$. Then, bring $v_z = c\rho_z/\rho - q\rho_z/\rho^2$ and $v_{zz} = [(c\rho - q)/\rho^2]\rho_{zz}$ into Eq. (25) and rewrite the resulting equation, then the following equation is obtained:

$$\rho_{zz} + \frac{2}{(\lambda + M)\Delta^2}\left(\frac{q_*}{\rho} - \lambda\Delta - M\Delta\right)\rho_z + \frac{2\rho(v_e(\rho)\rho - c\rho - q_*)}{T(\lambda + M)\Delta^2 q_*} = 0. \tag{26}$$

The second-order ordinary differential equation can be obtained by the simplification $\rho_{zz} - G(\rho, q_*)\rho_z - F(\rho, c, q_*) = 0$, in which

$$G(\rho, q_*) = \frac{2}{(\lambda + M)\Delta^2}\left(\frac{q_*}{\rho} - \lambda\Delta - M\Delta\right), \tag{27}$$

$$F(\rho, c, q_*) = \frac{-2\rho}{T(\lambda + M)\Delta^2 q_*}[q_* + c\rho - \rho V_e(\rho)]. \tag{28}$$

Let $y = \mathrm{d}\rho/\mathrm{d}z$, then equation (25) can be transformed into a system of first-order ordinary differential equations as follows:

$$\begin{cases} \dfrac{\mathrm{d}\rho}{\mathrm{d}z} = y, \\ \dfrac{\mathrm{d}y}{\mathrm{d}z} = G(\rho, q_*)y + F(\rho, c, q_*). \end{cases} \tag{29}$$

Then, for the type of equilibrium point and its stability, it is mainly determined by a system of equations composed of Eq. (29). Let the terms on the right-hand side of Eq. (25) be 0, then $y = 0$ and $F = 0$, from which the coordinates of equilibrium point (a, b) can be obtained. Therefore, the linear representation of the system can be obtained by Taylor expansion of Eq. (29) according to the coordinates of the equilibrium point:

$$\begin{cases} \rho' = y, \\ y' = G(\rho_i, q_*)y + F'(\rho_i, c, q_*)(\rho - \rho_i). \end{cases} \tag{30}$$

Thus, the Jacobian matrix of the system at the equilibrium point is $\boldsymbol{L} = \begin{bmatrix} 0 & 1 \\ F_i' & G_i \end{bmatrix}$. The corresponding characteristic equation is $\lambda^2 - G_i\lambda - F_i' = 0$, where $G_i(\rho_i, c, q_*) = G(\rho, c, q_*)$ and $\mathrm{F}' = F(\rho, c, q_*)$, and specifically

$$G_{\mathrm{i}} = \frac{2}{(\lambda + M)\Delta^2}\left(\frac{q_*}{\rho} - \lambda\Delta - M\Delta\right), \tag{31}$$

$$F_{\mathrm{i}}' = \frac{-2\rho_i}{T(\lambda + M)\Delta^2 q_*}[c - \rho_i V_{\mathrm{e}}'(\rho_i) - V_{\mathrm{e}}(\rho_i)]. \tag{32}$$

Since at the equilibrium point $(\rho_i, 0)$, $F = 0$, then $q_* + c\rho_i - \rho_i V_{\mathrm{e}}(\rho_i) = 0$, thus F_i' can be written as

$$F_i' = \frac{-2(q_* + \rho_i^2 V_{\mathrm{e}}'(\rho_i))}{T(\lambda + M)\Delta^2 q_*}.$$

According to the qualitative theory of differential equations, the equilibrium point type of linear system (30) can be determined as follows: (i) when $F_i' > 0$, the equilibrium point is a saddle point; (ii) when $G_i^2 + 4F_i' > 0$ and $F_i' < 0$, the equilibrium point is a node; (iii) when $G_i^2 + 4F_i' < 0$ and $G_i \neq 0$, the equilibrium point is a focus; (iv) when $F_{\mathrm{i}}' < 0$ and $G_i = 0$, the equilibrium point is the center. When $z \to \pm\infty$, the stability of the linear system at the saddle point is unstable; when $G_i < 0$ (or $G_i > 0$), the stability at the node and focal point, for $z \to +\infty$ (or $z \to -\infty$) is stable.

From the Hartman–Gorban linearization theorem, the nonlinear system (29) and the linear system (39) have the same equilibrium point. For the equilibrium point that is not the center, the stability at the equilibrium point is the same for the nonlinear system (29) and the linear system (39). Given any set of traveling wave velocity c and traveling wave parameter q_*, the equilibrium points ρ_1, ρ_2, ρ_3 of the linear system (29) can be solved. Select the equilibrium velocity function proposed in Ref. [39]:

$$V_{\mathrm{e}}[\rho] = v_{\mathrm{f}}\left\{\left[1 + \exp\left(\frac{\rho/\rho_{\mathrm{m}} - 0.25}{0.06}\right)\right]^{-1} - 3.72 \times 10^{-6}\right\}, \tag{33}$$

where v_{f} represents the free flow velocity, and ρ_{m} denotes the maximum or congestion density.

The parameters in the model in this section are obtained by referring to relevant literature in the same field, and their values are as follows:[40,41] free flow velocity $v_{\mathrm{f}} = 30$ m/s, congestion density $\rho_{\mathrm{m}} = 0.2$ veh/m, driver's reaction time $T = 10$ s, disturbance propagation speed $c_0 = 11$ m/s, and viscosity coefficient $\mu_0 = 550$. When ρ is equal to 0, this is a trivial equilibrium point and has no practical meaning, so only other equilibrium points need discussing. From the above discussion and Eqs. (29) and (30), the type and stability of the equilibrium point can be judged as shown in Table 1, where the equilibrium point is represented by ρ_i $(i = 1, 2, 3)$.

Table 1. Equilibrium point type and its stability when model parameters are given, where $\Delta_{\mathrm{i}} = G_i^2 + 4F_i'$, $i = 1, 2, 3$.

c (m·s^{-1}), q_* (veh·s^{-1})	ρ_1 (veh·m^{-1})	ρ_2 (veh·m^{-1})	ρ_3 (veh·m^{-1})
$(c, q_*) = (-1.371, 0.2)$	0.0065 $F_i' > 0$, saddle point unstable for $z \to \pm\infty$	0.0938 $\Delta_i < 0$, $G_i < 0$, spiral point unstable for $z \to +\infty$ stable for $z \to -\infty$	0.1447 $F_i' > 0$, saddle point stable for $z \to \pm\infty$
$(c, q_*) = (-1.38, 0.64)$	0.0223 $F_i' > 0$, saddle point stable for $z \to \pm\infty$	0.0594 $\Delta_i < 0$, $G_i < 0$, spiral point unstable for $z \to +\infty$ stable for $z \to -\infty$	

Two groups of parameters in Table 2 are selected to simulate the stability of the nonlinear system (29) at the equilibrium point. The phase plane near the equilibrium point is shown

in Figs. 1 and 2, where the equilibrium point is $(\rho_i, 0)$, with $i = 1,2,3$ and $\rho_1 < \rho_2 < \rho_3$. It can be seen from the figures that the type of equilibrium point and the stability change near the equilibrium point of the system are consistent with the theoretical analysis results.

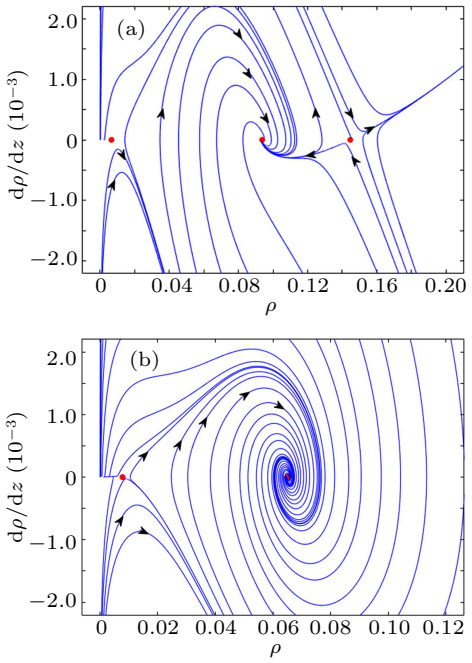


Fig. 3. Phase planes in the vicinity of model's equilibrium point for (a) $c = -1.371$ and $q_* = 0.2$ and (b) $c = -1.38$ and $q_* = 0.64$.

Figure 3(a) corresponds to the first case in Table 1. It can be seen from Table 1 that when $z \to \pm\infty$, the system is unstable at the equilibrium points $(\rho_1, 0)$ and $(\rho_2, 0)$, and the nearby tracks are far from this point. When $z \to +\infty$, there are several spiral trajectories close to the saddle point $(\rho_2, 0)$ and tend to focus $(\rho_3, 0)$, when $z \to -\infty$, these trajectories move away from the focus and eventually tend to infinity. The results show that the system is stable at $(\rho_3, 0)$ when $z \to +\infty$, the system is unstable at $(\rho_3, 0)$ when $z \to -\infty$, and the trajectory can be regarded as the saddle point focus saddle point solution of the system.

Figure 3(b) corresponds to the second case in Table 1. Figure 3(b) also shows that the system is unstable at the equilibrium point $(\rho_2, 0)$. At $z \to +\infty$, the spiral trajectory tends to focus $(\rho_1, 0)$, and the system is stable at this point, when $z \to -\infty$, the spiral trajectory is far from the focus $(\rho_1, 0)$, and the system is unstable.

5. Bifurcation analysis considering full speed difference model

5.1. Derivation of Hopf bifurcation existence condition considering full speed difference model

Lemma 1[42] Consider the system $\boldsymbol{X} \in R^n$, $\dot{x} = \boldsymbol{f}(\boldsymbol{x}, \lambda)$, and $\lambda \in R$, with λ serving as variable parameter. If the equilibrium point $\boldsymbol{f}(\boldsymbol{x}, l)\big|_{(x_0, l_0)} = 0_{n\times 1}$ is satisfied, then $\boldsymbol{L} = D_x \boldsymbol{f}(\boldsymbol{x}, \lambda)\big|_{(x_0, \lambda_0)}$, and its eigenvalue is $\alpha(\lambda) \pm \mathrm{i}\beta(\lambda)$, if $\alpha(\lambda_0) = 0$ and $\beta(\lambda_0) = \omega > 0$, $c = \dot{a}(\lambda)\big|_{\lambda_0} \neq 0$, then the system has a Hopf bifurcation at $\lambda = \lambda_0$.

For system (29), let q_* be a variable parameter which has an equilibrium point $(\eta_0, 0)$ for any value of q_*, and the derivative matrix at the equilibrium point is

$$\boldsymbol{L}(q_*) = \left(\begin{array}{cc} 0 & 1 \\ \dfrac{-2\rho_i}{T(\lambda+M)\Delta^2 q_*}[c - \rho_i V_e'(\rho_i) - V_e(\rho_i)] & \dfrac{2}{(\lambda+M)\Delta^2}\left(\dfrac{q_*}{\rho} - \lambda\Delta - M\Delta\right) \end{array} \right)\Bigg|_{\substack{\rho=\rho_0 \\ q^*=q_0^*}} \triangleq \begin{pmatrix} b_1 & b_2 \\ b_3 & b_4 \end{pmatrix}. \tag{34}$$

Let its eigenvalue be λ, $\lambda = R(q_*) \pm \mathrm{j}I(q_*)$, then its characteristic equation will be

$$\lambda^2 - (b_1 + b_4)\lambda + (b_1 b_4 - b_2 b_3) = 0. \tag{35}$$

Let the pair of eigenvalues of this equation be $R(q_*) \pm \mathrm{j}I(q_*)$, then the following results will be obtained:

$$R(q_*) = \frac{b_1 + b_4}{2} = \frac{1}{(\lambda+M)\Delta^2}\left(\frac{q_*}{\rho} - \lambda\Delta - M\Delta\right), \tag{36}$$

$$\begin{aligned} I(q_*) &= \sqrt{(b_1 b_4 - b_2 b_3) - \frac{(b_1 + b_4)^2}{4}} \\ &= \sqrt{-\frac{-2\rho_i}{T(\lambda+M)\Delta^2 q_*}[c - \rho_i V_e'(\rho_i) - V_e(\rho_i)] - \left(\frac{1}{(\lambda+M)\Delta^2}\left(\frac{q_*}{\rho} - \lambda\Delta - M\Delta\right)\right)^2}, \end{aligned} \tag{37}$$

$$c = R'(q_*)\big|_{q_{*0}} = \frac{1}{(\lambda+M)\Delta^2} \neq 0. \tag{38}$$

Order $R(\rho_0, q_{*0}) = 0$, then

$$R(\rho_0, q_{*0}) = \left(\left(q_*/\rho - \lambda\Delta - M\Delta\right)\right)\big|_{q_* = q_{*0}} \triangleq 0. \tag{39}$$

Thus, we have

$$q_{*0} = (\lambda + M)\Delta\rho_0. \tag{40}$$

Also the following expression is available at the same time:

$$I(q_*) = \sqrt{(b_1b_4 - b_2b_3) - \frac{(b_1+b_4)^2}{4}}$$
$$= \sqrt{-\frac{-2\rho_i}{T(\lambda+M)\Delta^2 q_*}[c - \rho_i V_e'(\rho_i) - V_e(\rho_i)] - \left(\frac{1}{(\lambda+M)\Delta^2}\left(\frac{q_*}{\rho} - \lambda\Delta - M\Delta\right)\right)^2}. \quad (41)$$

Since $F = 0$ at the equilibrium point, it follows that $q_* + c\rho_i - \rho_i V_e(\rho_i) = 0$, F_i' can be written as

$$F_i' = \frac{2(q_* + \rho_i^2 V_e(\rho_i))}{T(\lambda+M)\Delta^2 q_*}. \quad (42)$$

From Eq. (40) it follows that

$$I(\rho_0, q_*) = \sqrt{\frac{2(q_* + \rho_i^2 V_e(\rho_i))}{T(\lambda+M)\Delta^2 q_*}}\Bigg|_{\substack{\rho=\rho_0 \\ q_*=q_{*0}}}. \quad (43)$$

Since $V_e'(\rho) < 0$, when $-\rho_0^2 V_e(\rho_0) > q_{*0} > 0$. At this point, $I(\rho_0, q_{*0}) > 0$ there is a Hopf bifurcation in the system at $q_* = q_{*0}$.

5.2. Derivation of existence conditions for saddle intersection bifurcation for macro traffic flow modeling

Lemma 2[42] Consider the system $x' = \boldsymbol{f}(\boldsymbol{x}, \lambda)$, $\boldsymbol{x} \in R^n$, $\lambda \in R$, λ serving as a variable parameter. If (x_0, λ) satisfies the equilibrium point condition $\boldsymbol{f}(\boldsymbol{x}, \lambda)\big|_{(x_0,\lambda_0)} = \boldsymbol{0}_{n\times 1}$, then $\boldsymbol{L} = D_x \boldsymbol{f}(\boldsymbol{x}, \lambda)\big|_{(x_0,\lambda_0)}$, is taken. And let ψ and ϕ be the left unit eigenvector and the right unit eigenvector of $\boldsymbol{L}$, i.e., $\psi \boldsymbol{L} = 0$ and $\boldsymbol{L}\phi = 0$, respectively, then $\lambda = \lambda_0$ will be a saddle-knotted bifurcation of the system when the following condition is satisfied:

i) $a = \psi \cdot \dfrac{\partial}{\partial \lambda} \boldsymbol{f}(\boldsymbol{x}, \lambda)\big|_{(x_0,\lambda_0)} \neq 0,$ (44)

ii) $b = \psi \cdot \sum_{i=1}^{n} e_i [\phi^{\mathrm{T}} \dfrac{\partial^2}{\partial \boldsymbol{x}^2} \boldsymbol{f}_i(\boldsymbol{x}, \lambda)\big|_{(x_0,\lambda_0)} \phi] \neq 0.$ (45)

Then for any small $\varepsilon > 0$, the approximate expression of the solution curve around (x_0, λ_0) is

$$x = \varepsilon\phi + o(\varepsilon^2), \quad \lambda = \frac{\varepsilon^2 b}{2a} + o(\varepsilon^3). \quad (46)$$

For system (29), let q_* be a variable parameter, then the derivative matrix at the equilibrium point will be expressed in Eq. (47). When $q_{*0} = -\rho_0^2 V_e'(\rho_0)$, there exists $\phi = \begin{pmatrix} 1 \\ 0 \end{pmatrix}$ satisfying $\boldsymbol{L}\phi = 0$. At this time,

$$\psi \boldsymbol{L} = \boldsymbol{0} \Rightarrow \psi = \begin{pmatrix} \dfrac{2}{(\lambda+M)\Delta^2}\left((\lambda+M)\Delta - \dfrac{q_{*0}}{\rho_0}\right) & 1 \end{pmatrix}. \quad (47)$$

Substituting the variables ψ and ϕ into Eqs. (44) and (45), the following results can be obtained

$$a = \psi \cdot \frac{\partial}{\partial q_*} \boldsymbol{f}(\boldsymbol{x}, q_*)\Big|_{(x_0,q_{*0})}$$
$$= \begin{pmatrix} \dfrac{2}{(\lambda+M)\Delta^2}\left((\lambda+M)\Delta - \dfrac{q_{*0}}{\rho_0}\right) & 1 \end{pmatrix} \times \begin{pmatrix} 0 \\ -\dfrac{2\rho_0}{T(\lambda+M)\Delta^2 q_{*0}} \end{pmatrix}$$
$$= -\frac{2\rho_0}{T(\lambda+M)\Delta^2 q_{*0}} \neq 0. \quad (48)$$

Then

$$b = \psi \cdot \sum_{i=1}^{n} e_i \left[\phi^{\mathrm{T}} \frac{\partial^2}{\partial \boldsymbol{x}^2} \boldsymbol{f}_i(\boldsymbol{x}, \lambda)\big|_{(x_0,\lambda_0)} \phi\right] = \begin{pmatrix} \dfrac{2}{(\lambda+M)\Delta^2}\left((\lambda+M)\Delta - \dfrac{q_{*0}}{\rho_0}\right) & 1 \end{pmatrix}$$
$$\times \begin{pmatrix} \begin{pmatrix} 1 & 0 \end{pmatrix} \begin{pmatrix} 0 & 0 \\ 0 & 0 \end{pmatrix} \begin{pmatrix} 1 \\ 0 \end{pmatrix} \\ \begin{pmatrix} 1 & 0 \end{pmatrix} \begin{pmatrix} \dfrac{4V_e(\rho_0) + 8\rho_0 V_e'(\rho_0) + 2\rho_0^2 V_e''(\rho_0) - 4c}{T(\lambda+M)\Delta^2 q_{*0}} & -\dfrac{2q_*}{(\lambda+M)\Delta^2\rho_0^2} \\ -\dfrac{2q_*}{(\lambda+M)\Delta^2\rho_0^2} & 0 \end{pmatrix} \begin{pmatrix} 1 \\ 0 \end{pmatrix} \end{pmatrix}$$
$$= \frac{4V_e(\rho_0) + 8\rho_0 V_e'(\rho_0) + 2\rho_0^2 V_e''(\rho_0) - 4c}{T(\lambda+M)\Delta^2 q_{*0}} \neq 0. \quad (49)$$

So when $q_{*0} = -\rho_0^2 V_e'(\rho_0)$, system (29) has a saddle-junction-type bifurcation at $q_* = q_{*0}$.

5.3. Consider Hopf bifurcation type for full velocity difference model

For the Hopf bifurcation problem, since the n-dimensional system can be restricted to a two-dimensional central manifold by the central manifold method, herein only the Hopf bifurcation of the two-dimensional system is considered.

Lemma 3[42] The parameters of a two-dimensional systemare assumed as follows:

$$\boldsymbol{x}' = \boldsymbol{f}(\boldsymbol{x},\gamma) \quad \boldsymbol{x} = (x_1,x_2)^{\mathrm{T}} \in R^2, \quad \gamma \in R. \tag{50}$$

The equilibrium point of the system is the origin $O(0,0)$, and the eigenvalues at the origin are $\alpha(\gamma) \pm \mathrm{i}\omega(\gamma)$. Also $\gamma = 0$, when the partial derivative matrix of the system has pure imaginary eigenvalue $\mathrm{i}\omega_0$, that is, $\alpha(0) = 0, \omega(0) = \omega_0 > 0$. By taking the coordinate transformation, the system (50) can be written as

$$\begin{cases} x_1' = \alpha(\gamma)x_1 - \omega(\gamma)x_2 + \tilde{f}_1(x_1,x_2,\gamma), \\ x_2' = \omega(\gamma)x_1 + \alpha(\gamma)x_2 + \tilde{f}_2(x_1,x_2,\gamma), \end{cases} \tag{51}$$

which $\tilde{f}_1, \tilde{f}_2 = O(x_1^2 + x_2^2)$.

Theorem 1 (Hopf bifurcation theorem for models) Let the partial derivative matrix $D(\gamma)$ of system (50) at the origin have eigenvalues $\alpha(\gamma) \pm \mathrm{i}\omega(\gamma)$, and satisfy $\alpha(0) = 0, \omega(0) = \omega_0 > 0$, and $c = \alpha'(0) \neq 0$, then there will exist an analytic function $\gamma(\varepsilon) = \sum\limits_{k=2}^{\infty} \gamma_k \varepsilon^k$ such that for $\gamma = \gamma(\varepsilon) \neq 0$. The system (43) has a unique closed orbit in a sufficiently small neighborhood of the origin Γ_ε, whose period is

$$T(\varepsilon) = \frac{2\pi}{\omega_0}\left(1 + \sum_{k=2}^{\infty} \tau_k \varepsilon^k\right). \tag{52}$$

When $\varepsilon \to 0$ and $\gamma(\varepsilon) \to 0$, Γ_ε converges to the origin. Let γ_{k1} be the coefficient of the first term in the analytic function $\gamma(\varepsilon) = \sum_{k=2}^{\infty} \gamma_k \varepsilon^k$ that is not equal to zero, then Γ_ε will be an unstable limit ring when γ_{k1} and c have the same sign, and Γ_ε will be an unstable limit ring when γ_{k1} and c have different signs.

The proof of Theorem 1 and the formula γ_k, τ_k for the coefficients can be found in Ref. [42], especially when $k = 2$:

$$\gamma_2 = -a/c, \tau_2 = -\left(b + \gamma_2\omega'(0)\right)/\omega_0, \tag{53}$$

in which

$$\begin{aligned} a = {} & (1/16)\left[\tilde{f}_{1xxx} + \tilde{f}_{1xyy} + \tilde{f}_{2xxy} + \tilde{f}_{2yyy}\right] \\ & + (1/16\omega_0)\left[\tilde{f}_{1xy}\left(\tilde{f}_{1xx} + \tilde{f}_{1yy}\right) - \tilde{f}_{2xy}\left(\tilde{f}_{2xx} + \tilde{f}_{2yy}\right)\right. \\ & \left. - \tilde{f}_{1xx}\tilde{f}_{2xx} + \tilde{f}_{1yy}\tilde{f}_{2yy}\right], \end{aligned} \tag{54}$$

where $\tilde{f}_{1xxx}$ and $\tilde{f}_{2xxx}$ are the partial derivatives at (0, 0, 0), a is an important parameter to judge the stability of the limit ring. Assuming that the conditions of Theorem 1 hold, the following stability conclusion is drawn according to the Hopf bifurcation:

(i) If $a < 0\,(> 0)$, then the limit ring Γ_ε is stable (unstable);

(ii) If a and c have different signs (same sign), then the Hopf bifurcation is supercritical (subcritical);

(iii) If $a = 0$, then the Hopf bifurcation is degenerate.

For system (29), let q_* be a variable parameter which has an equilibrium point $(\rho_0, 0)$ for any value of q_*, and let $\tilde{\rho} = \rho - \rho_0$, translate the coordinates and move the equilibrium point to the origin, at which point the system can be expressed as follows:

$$\begin{cases} \tilde{\rho}' = y, \\ y' = \dfrac{2}{(\lambda+M)\Delta^2}\left(\dfrac{q_*}{\tilde{\rho}+\rho_0} - (\lambda+M)\Delta\right)y - \dfrac{2(\tilde{\rho}+\rho_0)}{T(\lambda+M)\Delta^2 q_*}\left[q_* + c(\tilde{\rho}+\rho_0) - (\tilde{\rho}+\rho_0)V_{\mathrm{e}}(\tilde{\rho}+\rho_0)\right]. \end{cases} \tag{55}$$

By performing a Taylor expansion at the equilibrium point $(\tilde{\rho}, y) = (0,0)$, the system can be linearized as $\tilde{\boldsymbol{x}}' = \boldsymbol{L}(q_*)\tilde{\boldsymbol{x}} + \boldsymbol{f}$, where $\boldsymbol{f}$ is a smooth vector function whose components $\boldsymbol{f}_{1,2}$ are the Taylor expansions of the least quadratic terms about $\tilde{x}$, which can be expressed as follows:

$$\boldsymbol{f} = \begin{bmatrix} 0 \\ k_{11}\tilde{\rho}^2 + k_{22}y^2 + k_{12}\tilde{\rho}y + k_{111}\tilde{\rho}^3 + k_{222}y^3 + k_{112}\tilde{\rho}^2 y + k_{122}\tilde{\rho}y^2 + O(\tilde{\rho},y)^4 \end{bmatrix}. \tag{56}$$

The Jacobi matrix $\boldsymbol{L}(q_*)$ can be expressed as

$$\boldsymbol{L}(q_*) = \left(\begin{matrix} 0 & 1 \\ \dfrac{-2\rho_i}{T(\lambda+M)\Delta^2 q_*}[c - \rho_i V_{\mathrm{e}}'(\rho_i) - V_{\mathrm{e}}(\rho_i)] & \dfrac{2}{(\lambda+M)\Delta^2}\left(\dfrac{q_*}{\rho} - \lambda\Delta - M\Delta\right) \end{matrix} \right)\Bigg|_{\substack{\rho=\rho_0 \\ q_*=q_{*0}}} \triangleq \begin{pmatrix} b_1 & b_2 \\ b_3 & b_4 \end{pmatrix}. \tag{57}$$

Its eigenvalues are the roots of the following characteristic equation:

$$\lambda^2 - \sigma\lambda + \Delta = 0, \tag{58}$$

of which, $\sigma = \sigma(q_*) = d(q_*) = \mathrm{tr}\,\boldsymbol{L}(q_*)$, $\Delta = \Delta(q_*) = -b(q_*) = \det \boldsymbol{L}(q_*)$,

$$\lambda_{1,2}(q_*) = \frac{1}{2}\left(\sigma(q_*) \pm \sqrt{\sigma^2(q_*) - 4\Delta(q_*)}\right). \tag{59}$$

From the Hopf bifurcation condition we have

$$\sigma(0)=0,\quad \Delta(0)=\omega_0^2>0. \tag{60}$$

For smaller variables, $|q_*|$ can be introduced in the form of

$$\alpha(q_*)=\frac{1}{2}\sigma(q_*),\quad \omega(q_*)=\frac{1}{2}\sqrt{4\Delta(q_*)-\sigma^2(q_*)}. \tag{61}$$

This leads to the following eigenvalue expressions:

$$\lambda_1(q_*)=\lambda(q_*),\quad \lambda_2(q_*)=\bar{\lambda}(q_*), \tag{62}$$

in which

$$\begin{aligned}&\lambda(q_*)=\alpha(q_*)+\mathrm{i}\omega(q_*),\\ &\alpha(0)=0,\quad \omega(0)=\omega_0>0.\end{aligned} \tag{63}$$

Let $\omega_{\mathrm{re}}+\mathrm{i}\omega_{\mathrm{im}}$ be the eigenvector $\boldsymbol{L}(q_*)$ corresponding to the eigenvalue $\lambda(q_*)$, with

$$\boldsymbol{L}(\omega_{\mathrm{re}}+\mathrm{i}\omega_{\mathrm{im}})=\mathrm{i}\omega_0(\omega_{\mathrm{re}}+\mathrm{i}\omega_{\mathrm{im}}). \tag{64}$$

Considering that the real part and the imaginary part on both sides of the above equation are equal, thus

$$\begin{cases}\boldsymbol{L}\omega_{\mathrm{im}}=\omega_0\omega_{\mathrm{re}},\\ \boldsymbol{L}\omega_{\mathrm{re}}=-\omega_0\omega_{\mathrm{im}}.\end{cases} \tag{65}$$

Equation (65) is rectified as follows:

$$\boldsymbol{L}[\omega_{\mathrm{im}}\omega_{\mathrm{re}}]=[\omega_{\mathrm{im}}\omega_{\mathrm{re}}]\begin{bmatrix}0&-\omega_0\\ \omega_0&0\end{bmatrix}. \tag{66}$$

From this

$$[\omega_{\mathrm{im}}\omega_{\mathrm{re}}]^{-1}\boldsymbol{L}[\omega_{\mathrm{im}}\omega_{\mathrm{re}}]=\begin{bmatrix}0&-\omega_0\\ \omega_0&0\end{bmatrix}, \tag{67}$$

ordering

$$\tilde{\boldsymbol{y}}=[\omega_{\mathrm{im}}\omega_{\mathrm{re}}]^{-1}\tilde{\boldsymbol{x}}, \tag{68}$$

yields the following expression:

$$\tilde{\boldsymbol{y}}'=[\omega_{\mathrm{im}}\omega_{\mathrm{re}}]^{-1}\tilde{\boldsymbol{x}}'. \tag{69}$$

Substituting the equation $\tilde{\boldsymbol{x}}'=\boldsymbol{L}(q_*)\tilde{\boldsymbol{x}}+\boldsymbol{f}$ into Eq. (69) obtains

$$\begin{aligned}\tilde{\boldsymbol{y}}' &= [\omega_{\mathrm{im}}\ \omega_{\mathrm{re}}]^{-1}\boldsymbol{L}[\omega_{\mathrm{im}}\ \omega_{\mathrm{re}}]\tilde{\boldsymbol{y}}+[\omega_{\mathrm{im}}\ \omega_{\mathrm{re}}]^{-1}\boldsymbol{f}\\ &= \begin{bmatrix}0&-\omega_0\\ \omega_0&0\end{bmatrix}\tilde{\boldsymbol{y}}+[\omega_{\mathrm{im}}\ \omega_{\mathrm{re}}]^{-1}\boldsymbol{f}.\end{aligned} \tag{70}$$

In addition, the eigenvectors of $\boldsymbol{L}(q_*)$ can be calculated as follows:

$$\omega_{\mathrm{re}}+\mathrm{i}\omega_{\mathrm{im}}=\begin{bmatrix}0\\1\end{bmatrix}+\mathrm{i}\begin{bmatrix}-\dfrac{1}{\sqrt{-b(q_*)}}\\ 0\end{bmatrix}. \tag{71}$$

Substituting Eq. (56) and the values of ω_{im} and ω_{re} into Eq. (59) yields

$$\tilde{\boldsymbol{y}}'=\begin{bmatrix}0&-\omega_0\\ \omega_0&0\end{bmatrix}\tilde{\boldsymbol{y}}+\begin{bmatrix}0\\ k_{11}\tilde{\rho}^2+k_{22}y^2+k_{12}\tilde{\rho}y+k_{111}\tilde{\rho}^3+k_{222}y^3+k_{112}\tilde{\rho}^2y+k_{122}\tilde{\rho}y^2+O(\tilde{\rho},y)^4\end{bmatrix}. \tag{72}$$

Equation (55) has the same form as Eq. (45), so that the value of a in Eq. (29) can be calculated according to Eq. (55) as follows:

$$\begin{aligned}a &= (1/16)\left[\tilde{f}_{2\tilde{y}_1\tilde{y}_1\tilde{y}_2}+\tilde{f}_{2\tilde{y}_2\tilde{y}_2\tilde{y}_2}\right]\\ &\quad+(1/16\omega_0)\left[-\tilde{f}_{2\tilde{y}_1\tilde{y}_2}\left(\tilde{f}_{2\tilde{y}_1\tilde{y}_1}+\tilde{f}_{2\tilde{y}_2\tilde{y}_2}\right)\right],\end{aligned} \tag{73}$$

further, the value of c can be calculated as follows:

$$c=\alpha'(0)=\frac{1}{2\mu_0\rho_0}>0. \tag{74}$$

Thus, for equation system (29), the Hopf bifurcation is supercritical when $a<0$ and subcritical when $a>0$.

5.4. Hopf bifurcation feedback controller design for macro traffic flow modeling

In this subsection, the analysis of the improved macro traffic flow system model begins with the bifurcation control, i.e., the feedback controller that modifies the bifurcation characteristics of the system, such as bifurcation going forward, backward or disappearing at the equilibrium point in the control system. Hopf bifurcation control mainly includes shifting the original bifurcation points of the system and controlling the magnitude of the limit loop amplitude. Thus, the effect of preventing or relieving traffic congestion is achieved.

By designing the feedback controller, the occurrence of Hopf bifurcation can be delayed and the limit loop amplitude can be controlled. That is to say, completely eliminating Hopf bifurcation without changing the system equilibrium point can be achieved by controlling the limit loop amplitude. Firstly, the Hopf bifurcation point is controlled, i.e., the bifurcation appearing at the equilibrium point in the control system is advanced or delayed. From the Hopf bifurcation existence condition in Subsection 3.2.2, it is known that point $q_*=0.2$ is an equilibrium point of the system when parameter is $(0.056904,\ 0)$, and the system will have Hopf bifurcation behavior at that point. In this subsection, the feedback controller is designed to delay or advance the Hopf bifurcation appearing at this equilibrium point.

For ease of derivation, equation (29) for the nonlinear system of traffic flow is reduced to the following form:

$$\frac{\mathrm{d}y}{\mathrm{d}z} = \frac{2}{(\lambda+M)\Delta^2}\left[\frac{q}{\rho}-\lambda\Delta-M\Delta\right]y + \frac{2(v_{\mathrm{e}}(\rho)-c)}{T(\lambda+M)\Delta^2 q_*}\rho^2 - \frac{2}{(\lambda+M)\Delta^2}\rho. \tag{75}$$

By replacing the density variable ρ_i in Eq. (75) with x, the system can be simplified into

$$\frac{\mathrm{d}y}{\mathrm{d}z} = Ay + Bx^2 + Cx. \tag{76}$$

Combined with the form of the variables in the system model (76), the feedbacks can be set to be

$$C(x,y) = k_1 x + k_2 y + k_3 x^2. \tag{77}$$

The controlled system after adding the feedback controller equation (i.e. Eq. (77)) becomes

$$\begin{cases} \dot{x} = y, \\ \dot{y} = (k_2+A)y + (B+k_3)x^2 + (k_1+C)x + D. \end{cases} \tag{78}$$

Let $\alpha = k_2 + A$ and $\beta = k_1 + C$, the stochastic system (78) is expanded by the orthogonal approximation as

$$\begin{cases} \dot{x}_0 = y_0, \\ \dot{y}_0 = \alpha y_0 + \dfrac{r\delta}{2}[x_1] + (b+k_3)X_0 + \beta x_0 \\ \qquad + \dfrac{A\delta}{2}[S_0] + A\left(k_4+\mu''\right)S_0 + D, \\ \qquad \cdots, \\ \dot{x}_4 = y_4, \\ \dot{y}_4 = \alpha y_4 + \dfrac{r\delta}{2}[x_4] + (b+k_3)X_4 + \beta x_4 \\ \qquad + \dfrac{A\delta}{2}[S_4] + A\left(k_4+\mu''\right)S_4 + D. \end{cases} \tag{79}$$

This yields a deterministic system equivalent to system (75). From the Hopf bifurcation analysis theory of equivalent systems in Subsection 5.3, it follows that system (79) undergoes Hopf bifurcation at $(0.056904, 0)$, corresponding to the controlled system (78) satisfying the following conditions:

$$\begin{cases} k_1 + r + \mu_{\mathrm{c}} = \dfrac{-\sqrt{3}\delta}{2}, \\ \alpha > 0, \\ k_1 + 2k_3 < 1, \end{cases} \Rightarrow \begin{cases} \mu_{\mathrm{c}} = \left(-k_1 - \dfrac{\sqrt{3}\delta}{2} - r\right), \\ -a < k_2, \\ k_1 + 2k_3 < 1. \end{cases} \tag{80}$$

Then, by controlling the values of parameters k_1, k_2, and k_3 in the nonlinear feedback controller $C(x,y) = k_1 x + k_2 y + k_3 x^2$, the Hopf bifurcation phenomenon of the stochastic system can be advanced or retarded.

5.5. Derivation of existence conditions for Bogdanov–Takens (BT) bifurcation of system

Consider the system $\boldsymbol{X} \in R^n$, $\dot{x} = \boldsymbol{f}(\boldsymbol{x},\lambda)$, and $\lambda \in R$, λ as variable parameters. If the equilibrium point $\boldsymbol{f}(\boldsymbol{x},l)\big|_{(x_0,l_0)} = \boldsymbol{0}_{n\times 1}$ is satisfied, denote $\boldsymbol{L} = D_x\boldsymbol{f}(\boldsymbol{x},\lambda)\big|_{(x_0,\lambda_0)}$, and its eigenvalue is $\alpha(\lambda) \pm \mathrm{i}\beta(\lambda)$, if $\alpha(\lambda_0) = 0$ and $\beta(\lambda_0) = \omega \neq 0$, then the system has a BT bifurcation at $\lambda = \lambda_0$.

According to the bifurcation theory of deterministic nonlinear dynamical systems: the sufficient and necessary conditions for the existence of BT branches of the system are as follows.

(i) There exists a pair of conjugate eigenvalues $\alpha(\lambda) \pm \mathrm{i}\beta(\lambda)$ in the Jacobian matrix.

(ii) The Jacobian matrix must have at least one zero real eigenvalue and a pair of purely imaginary eigenvalues, $\alpha(\lambda_0) = 0$ and $\beta(\lambda_0) = \omega \neq 0$.

(iii) The other eigenvalues of the Jacobian matrix have negative real parts.

For system (29), let q_* be a variable parameter which has an equilibrium point $(\eta_0, 0)$ for any value of q_*, and the derivative matrix at the equilibrium point is

$$\boldsymbol{L}(q_*) = \left(\begin{array}{cc} 0 & 1 \\ \dfrac{-2\rho_i}{T(\lambda+M)\Delta^2 q_*}[c - \rho_i V_{\mathrm{e}}'(\rho_i) - V_{\mathrm{e}}(\rho_i)] & \dfrac{2}{(\lambda+M)\Delta^2}\left(\dfrac{q_*}{\rho} - \lambda\Delta - M\Delta\right) \end{array}\right)\Bigg|_{\substack{\rho=\rho_0 \\ q*=q*_0}} \triangleq \begin{pmatrix} b_1 & b_2 \\ b_3 & b_4 \end{pmatrix}. \tag{81}$$

Let its eigenvalue be λ, $\lambda = R(q_*) \pm \mathrm{j}I(q_*)$, then its characteristic equation will be

$$\lambda^2 - (b_1+b_4)\lambda + (b_1 b_4 - b_2 b_3) = 0. \tag{82}$$

Let the pair of eigenvalues of this equation be $R(q_*) \pm \mathrm{j}I(q_*)$, then the following results can be obtained:

$$R(q_*) = \frac{b_1+b_4}{2} = \frac{1}{(\lambda+M)\Delta^2}\left(\frac{q_*}{\rho} - \lambda\Delta - M\Delta\right), \tag{83}$$

$$I(q_*) = \sqrt{(b_1 b_4 - b_2 b_3) - \frac{(b_1+b_4)^2}{4}} = \sqrt{-\frac{-2\rho_i}{T(\lambda+M)\Delta^2 q_*}[c - \rho_i V_{\mathrm{e}}'(\rho_i) - V_{\mathrm{e}}(\rho_i)] - \left(\frac{1}{(\lambda+M)\Delta^2}\left(\frac{q_*}{\rho} - \lambda\Delta - M\Delta\right)\right)^2}, \tag{84}$$

$$c = R'(q_*)\big|_{q_{*0}} = \frac{1}{(\lambda+M)\Delta^2} \neq 0. \tag{85}$$

Ordering $R(\rho_0, q_{*_0}) = 0$ yields

$$R(\rho_0, q_{*_0}) = \left(\left(\frac{q_*}{\rho} - \lambda\Delta - M\Delta\right)\right)\Big|_{q_*=q_{*_0}} \triangleq 0. \tag{86}$$

Thus

$$q_{*_0} = (\lambda+M)\,\Delta\rho_0. \tag{87}$$

Also the following equation is available at the same time

$$I(q_*) = \sqrt{(b_1b_4 - b_2b_3) - \frac{(b_1+b_4)^2}{4}} = \sqrt{-\frac{-2\rho_i}{T(\lambda+M)\Delta^2 q_*}[c - \rho_i V_{\mathrm{e}}'(\rho_i) - V_{\mathrm{e}}(\rho_i)] - \left(\frac{1}{(\lambda+M)\Delta^2}\left(\frac{q_*}{\rho} - \lambda\Delta - M\Delta\right)\right)^2}. \tag{88}$$

From $F = 0$ at the equilibrium point, it follows that $q_* + c\rho_i - \rho_i V_{\mathrm{e}}(\rho_i) = 0$, and F_i' can be written as

$$F_i' = \frac{2(q_* + \rho_i^2 V_{\mathrm{e}}(\rho_i))}{T(\lambda+M)\Delta^2 q_*}. \tag{89}$$

From Eqs. (87) and (88) it follows that

$$I(\rho_0, q_*) = \sqrt{\frac{2(q_* + \rho_i^2 V_{\mathrm{e}}(\rho_i))}{T(\lambda+M)\Delta^2 q_*}}\Bigg|_{\substack{\rho=\rho_0 \\ q_*=q_{*_0}}}. \tag{90}$$

Because of $V_{\mathrm{e}}'(\rho) < 0$, when $q_{*_0} = c_0\rho_0$, $\alpha(\rho_0, q_{*_0}) = 0$, and when $-\rho_0^2 V_{\mathrm{e}}'(\rho_0) \neq q_{*_0}$, $\beta(\rho_0, q_{*_0}) \neq 0$. At this point, $I(\rho_0, q_{*_0}) > 0$ and there is a BT bifurcation in the system at $q_* = q_{*_0}$.

5.6. Derivation of joint KdV–mKdV equation for model

In this subsection, the nonlinear properties of the traffic flow are analyzed by using an approximate uptake method that considers coarse-grained long-wave modes. We focus on studying the system behavior under the nearly neutral stability condition of the system. We introduce a slow scale for the spatial variable$X$ and the temporal variable T : $\begin{cases} X = \varepsilon(x - bt) \\ T = \varepsilon^3 t \end{cases}$. Traffic flow density and speed are set to be

$$\begin{cases} \rho = \rho_0 + \varepsilon^2\hat{\rho}(X,T), \\ u = u_0 + \varepsilon^2\hat{u}(X,T). \end{cases} \tag{91}$$

Substituting Eq. (91) into Eq. (11), performing a Taylor expansion and retaining up to the fifth order of ε, we derive the following nonlinear partial differential equation:

$$\begin{aligned}
&\varepsilon^2 a(\hat{u} - \hat{\rho}u_{\mathrm{e}}') \\
&+\varepsilon^3\left[(u_0 + (1-p)\rho_0 u_{\mathrm{e}}' - \lambda\Delta - b)\partial_X\hat{u} + (1-p)u_0u_{\mathrm{e}}'\partial_X\hat{\rho}\right] \\
&+\varepsilon^4\Bigg[\hat{\rho}\hat{u} - \hat{\rho}^2u_{\mathrm{e}}' - \frac{1}{2}a\hat{\rho}^2u_{\mathrm{e}}'' \\
&-\frac{1}{2}\left[\lambda - (\lambda - ap\beta\tau\rho^2u_{\mathrm{e}}'(\rho))\right]\frac{\Delta^2}{2}\partial_X^2\hat{u}\Bigg] \\
&+\varepsilon^5\left[\partial_T\hat{u} + (\hat{u} + (1-p)(\rho_0\hat{\rho}u_{\mathrm{e}}'' + \hat{\rho}u_{\mathrm{e}}'))\partial_X\hat{u}\right. \\
&\left.+(1-p)(u_0\hat{\rho}u_{\mathrm{e}}'' + \hat{u}u_{\mathrm{e}}')\partial_X\hat{\rho}\right] = 0.
\end{aligned} \tag{92}$$

According to the second-order term of ε in Eq. (92), we obtain $\hat{u} = \hat{\rho}\hat{u}_{\theta_n(t)} + O(\varepsilon^2)$. On the basis of the third-order term of ε in Eq. (92), we consider $\rho_0\hat{u}_{\theta_n(t)} + u_0 - b = 0$. With Eq. (92) and $\hat{u} = \hat{\rho}\hat{u}_{\theta_n(t)} + O(\varepsilon^2)$, the third-order term of ε in $\rho_0\hat{u}_{\theta_n(t)} + u_0 - b = 0$ can be rewritten as

$$\begin{aligned}
&u_{\mathrm{e}}'\left(u_0 + a\rho_0u_{\mathrm{e}}' + \lambda\Delta u_0 - \lambda\Delta - u_0 - \rho_0u_{\mathrm{e}}'\right)\partial_X\hat{\rho} \\
&= \theta\varepsilon^2\partial_X\hat{\rho}.
\end{aligned} \tag{93}$$

Therefore, equation (92) can be rewritten as

$$\begin{aligned}
&\varepsilon^2 a(\hat{u} - \hat{\rho}u_{\mathrm{e}}') \\
&+\varepsilon^3\left[(u_0 + (1-p)\rho_0u_{\mathrm{e}}' - \lambda\Delta - b)\partial_X\hat{u} + (1-p)u_0u_{\mathrm{e}}'\partial_X\hat{\rho}\right] \\
&+\varepsilon^4\Bigg[\hat{\rho}\hat{u} - \hat{\rho}^2u_{\mathrm{e}}' - \frac{1}{2}a\hat{\rho}^2u_{\mathrm{e}}'' \\
&-\frac{1}{2}\left[\lambda - (\lambda - ap\beta\tau\rho^2u_{\mathrm{e}}'(\rho))\right]\frac{\Delta^2}{2}\partial_X^2\hat{u}\Bigg] \\
&+\varepsilon^5\left[\partial_T\hat{u} + (\hat{u} + a(\rho_0\hat{\rho}u_{\mathrm{e}}'' + \hat{\rho}u_{\mathrm{e}}'))\partial_X\hat{u}\right. \\
&\left.+(1-p)(u_0\hat{\rho}u_{\mathrm{e}}'' + \hat{u}u_{\mathrm{e}}')\partial_X\hat{\rho} + \theta\partial_X\hat{\rho}\right] = 0.
\end{aligned} \tag{94}$$

From the fourth-order term of ε in Eq. (94), we obtain

$$\begin{aligned}
\hat{\rho}\hat{u} &= u_{\mathrm{e}}'\hat{\rho}^2 + \frac{1}{2}au_{\mathrm{e}}''\hat{\rho}^2 \\
&+\frac{1}{2}\left[\lambda - (\lambda - ap\beta\tau\rho^2u_{\mathrm{e}}'(\rho))\right]\frac{\Delta^2}{2}\partial_X^2\hat{u}.
\end{aligned} \tag{95}$$

Inserting Eq. (95) into the fifth-order term of ε in Eq. (11) yields

$$\begin{aligned}
&\partial_T\hat{\rho} - f_1\partial_X^3\hat{\rho} - f_2\hat{\rho}\partial_X\hat{\rho} \\
&+\varepsilon\left[-f_3\partial_X^2\hat{\rho} + f_4\partial_X^4\hat{\rho} + f_5\partial_X^2\hat{\rho}^2\right] = 0, \\
&f_1 = -\frac{\Delta^2}{2}(\lambda - (1-p)V_{\mathrm{e}}(\rho))u_{\mathrm{e}}'^2, \\
&f_2 = -\left(2u_{\mathrm{e}}' + au_{\mathrm{e}}''\right), \quad f_3 = \theta, \quad f_4 = 0, \\
&f_5 = -\frac{1}{2}\left[u_{\mathrm{e}}'^2 - (1-p)\left(\rho_0u_{\mathrm{e}}'u_{\mathrm{e}}'' + 2u_{\mathrm{e}}'^2 + u_0u_{\mathrm{e}}''\right)\right].
\end{aligned} \tag{96}$$

Therefore, the amplitude of the isolated wave solution is

$$\begin{aligned}
&\partial_T\hat{\rho} - f_1\partial_X^3\hat{\rho} - f_2\hat{\rho}\partial_X\hat{\rho} \\
&+\varepsilon\left[-f_3\partial_X^2\hat{\rho} + f_4\partial_X^4\hat{\rho} + f_5\partial_X^2\hat{\rho}^2\right] = 0, \\
&A = \frac{21f_1f_2f_3}{24f_1f_5 - 5f_2f_4}.
\end{aligned} \tag{97}$$

In order to derive the joint KdV–mKdV equation, the following setting is used:

$$\alpha = 2u_{\mathrm{e}}' + au_{\mathrm{e}}'',$$

$$\beta = \left(u_e'^2 - (1-p)\left(\rho_0 u_e' u_e'' + 2u_e'^2 + u_0 u_e''\right)\right),$$
$$\gamma = -\frac{1}{2}\left[\lambda - \left(\lambda - ap\beta\tau\rho^2 u_e'(\rho)\right)\right]\frac{\Delta^2}{2}. \quad (98)$$

Then the joint KdV–mKdV equation is expressed as $\partial_T\hat{\rho} + (\alpha + \beta\hat{\rho})\hat{\rho}\partial_X\hat{\rho} + \gamma\partial_X^3\hat{u} = 0$. One solution to the above joint KdV–mKdV equation is

$$\rho(x,t) = \frac{-\alpha}{2\beta}\left\{1 + \tanh\left[-\frac{\alpha^2}{24\beta\gamma}\left(x - \frac{\alpha^4}{144\beta^2\gamma}t\right)\right]\right. . \quad (99)$$

6. Numerical simulations

6.1. Macro traffic flow model bifurcation simulation

First, the initial value of the parameter q_* is selected to be 0.2, and the actual calculation direction of q_* is about $-30 \to 30$. In the bifurcation diagram, there are three bifurcation points in the figure, namely one Hopf (H) bifurcation points and two limit points (LPs). Figure 4 shows a bifurcation diagram with the appropriate parameters for q_*.

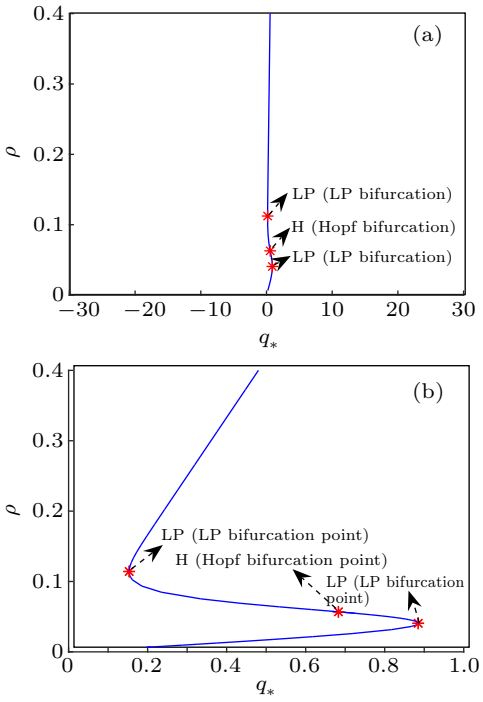


Fig. 4. Bifurcation diagram of $\rho - q_*$ for (a) a wide range of parameter q_* and (b) a suitable range of the parameter q_*.

If the limit point (LP) is selected as the starting point of the bifurcation calculation, the bifurcation calculation starting from this limit point will have a bifurcation type with a codimension of 2. At the same time, the activation parameters q_* and c are free parameters, and it can be found that the codimension is 2 bifurcations, such as Bogdanov–Takens (BT) bifurcation, cusp (CP) bifurcation, etc. The corresponding bifurcation diagrams are shown in Fig. 5.

When the parameter $c = -9.3370322$, and $q_* = 0.92428529$, the BT bifurcation is obtained, and the state variable of the BT bifurcation point is $(0.091434,\ 0.000000)$. When the parameter $c = -22.588037$, $q_* = 1.900569$, the CP bifurcation is obtained, and the state variable of the CP bifurcation point is $(0.060141,\ 0.000000)$. Below, we will continue to analyze the changes in the stability of the traffic system when the parameters pass through some of the bifurcation critical points calculated above. First, in order to study the influence of Hopf bifurcation on traffic flow, in this paper the stability change of the system in the phase plane is investigated when the parameter q_* passes through the point 0.46311827.

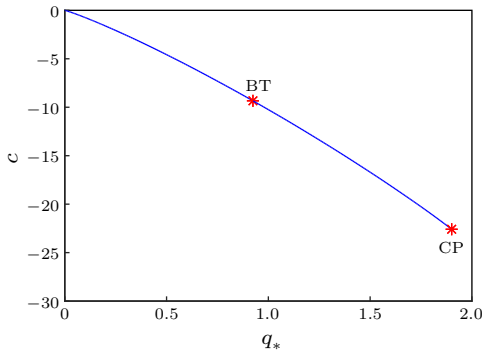


Fig. 5. Continuation solution diagram starting from limit point bifurcation: the bifurcation diagram with variables c and q_* as coordinates of vertical axis and horizontal axis.

Next, in this paper the influence of limit cycle bifurcations on traffic flow is studied when the parameter q_* passes through the point 0.17258763. First, consider the case of $q_* > 0.17258763$, and set $q_* = 0.18$. At this time, the system has two equilibrium points, i.e. a focal point (0.1017, 0) and a saddle point (0.1266, 0) as shown in Fig. 6. Therefore, the traffic system on the left side of the red line is stable, while the traffic system on the right side of the red line is unstable.

The red dashed line separates two different traffic flow scenarios, with the track on the left side of the dashed line approaching the stable focus and the track on the right side approaching infinity, indicating that with LP2 taken as the critical point, the traffic on the left side of LP2 tends to be in a free-flow state, while the right side of LP2 is constantly approaching the congested flow, and ultimately congested. The traffic system at this point can still be represented by synchronous flow. In the macro traffic flow model, q_* usually represents the maximum (or stable) traffic flow rate of the bottleneck section, also known as capacity. From the formula $-c\rho + q = \text{const} = q_*$, it can be seen that q_* also represents a flow difference, that is, the difference in flow between the positive flow q and the negative flow $c\rho$, which refers to the maximum traffic flow that the road can carry under certain conditions. When the traffic flow rate reaches q_*, the road will run in the best condition, further increase the traffic flow rate will lead to congestion and delay. Therefore, making good use of q_* can help planners and urban designers to better optimize road traffic management and improve urban traffic operation efficiency.

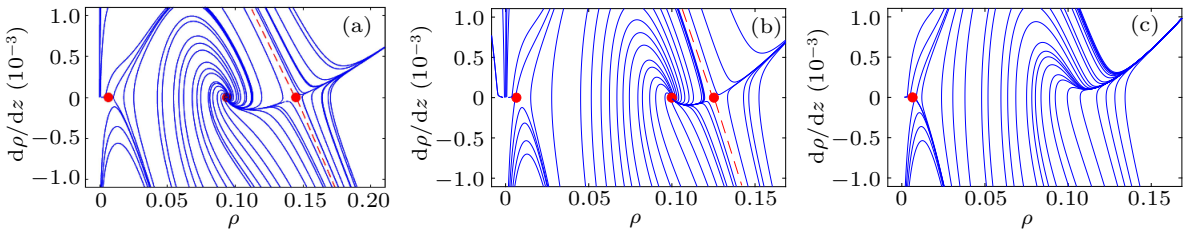


Fig. 6. Phase plane diagram of state change before and after the system has passed through saddle junction bifurcation for $q_* = 0.18$ (a), 0.17258763 (b), and 0.168 (c).

First, the change in the stability of the system when passing through the saddle-junction bifurcation point is analyzed as an example of the second saddle-junction bifurcation of the system. At this point, the system parameter $q_* = 0.17258763$. The change of the system state before and after passing through the saddle-junction bifurcation are shown in Fig. 6. Consider the case with $q_* > 0.17258763$, say, $q_* = 0.18$, as shown in Fig. 6(a). The system has three equilibrium points, i.e., a saddle junction point $(0.15119, 0)$, a focal point $(0.098651, 0)$, and another saddle junction point $(0.0058981, 0)$. The track inside the area on the left side of the red line keeps approaching the equilibrium point $(0.098651, 0)$. Therefore, the area on the left side of the red dashed line is stable, while the others are unstable. As the parameter q_* decreases, the red dashed line moves to the left and the area on the left side of the red dashed line decreases. When $q_* = 0.17258763$, a saddle node appears. When $q_* < 0.17258763$, say, $q_* = 0.16$, the equilibrium point in the system disappears and the whole system becomes unstable.

6.2. Improved Hopf bifurcation control simulation for macro traffic flow models

From the Subsection 5.4, it can be seen that by adjusting the values of parameters k_1, k_2, and k_3 in the nonlinear feedback controller $C(x, y) = k_1 x + k_2 y + k_3 x^2$, the Hopf bifurcation phenomenon of the stochastic system can be advanced or retarded. In the following, the control coefficient k_1 is taken for example and bifurcation diagrams for the controlled system are drawn to verify the role that the feedback controller plays.

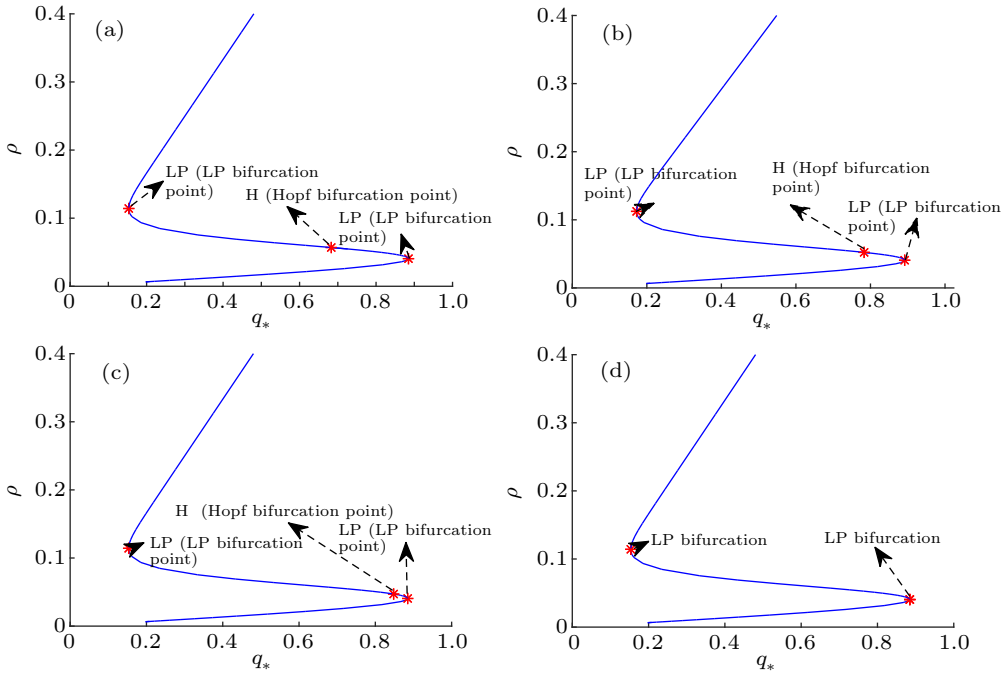


Fig. 7. System Hopf bifurcation movement diagrams for $k_1 = 0$ (a), 0.3 (b), 0.5 (c), and 0.8 (d), respectively.

When the system is not added to the control equation, the Hopf bifurcation occurs at the equilibrium point $(x, y) = (0.056904, 0)$. The bifurcation diagram of the system is drawn by substituting the relevant parameters as shown in Fig. 7. It can be seen from the figure that by adjusting the feedback controller, the Hopf bifurcation of the system is gradually delayed, and the Hopf bifurcation disappears when $k_1 = 0.8$. It is verified that the feedback controller designed by the bifurcation control method can eliminate or delay the occurrence of the Hopf bifurcation behavior of the stochastic system, and pre-

vent the stability of the traffic flow from changing abruptly due to the Hopf bifurcation, which causes the traffic system to enter the chaotic instability. By eliminating the unstable bifurcation phenomenon, traffic congestion can be induced and prevented in advance.

From Fig. 8(a), it can be seen that at this time the system is not subjected to feedback control. When $z \to +\infty$, the trajectory of the line in the graph converges to the focal point $(0.089061, 0)$, which indicates that the state of the system is stable at this equilibrium point; when $z \to -\infty$, the trajectory of the curve diverges at a distant position and produces oscillations with the same amplitude, indicating that the state of the system at this point is unstable.

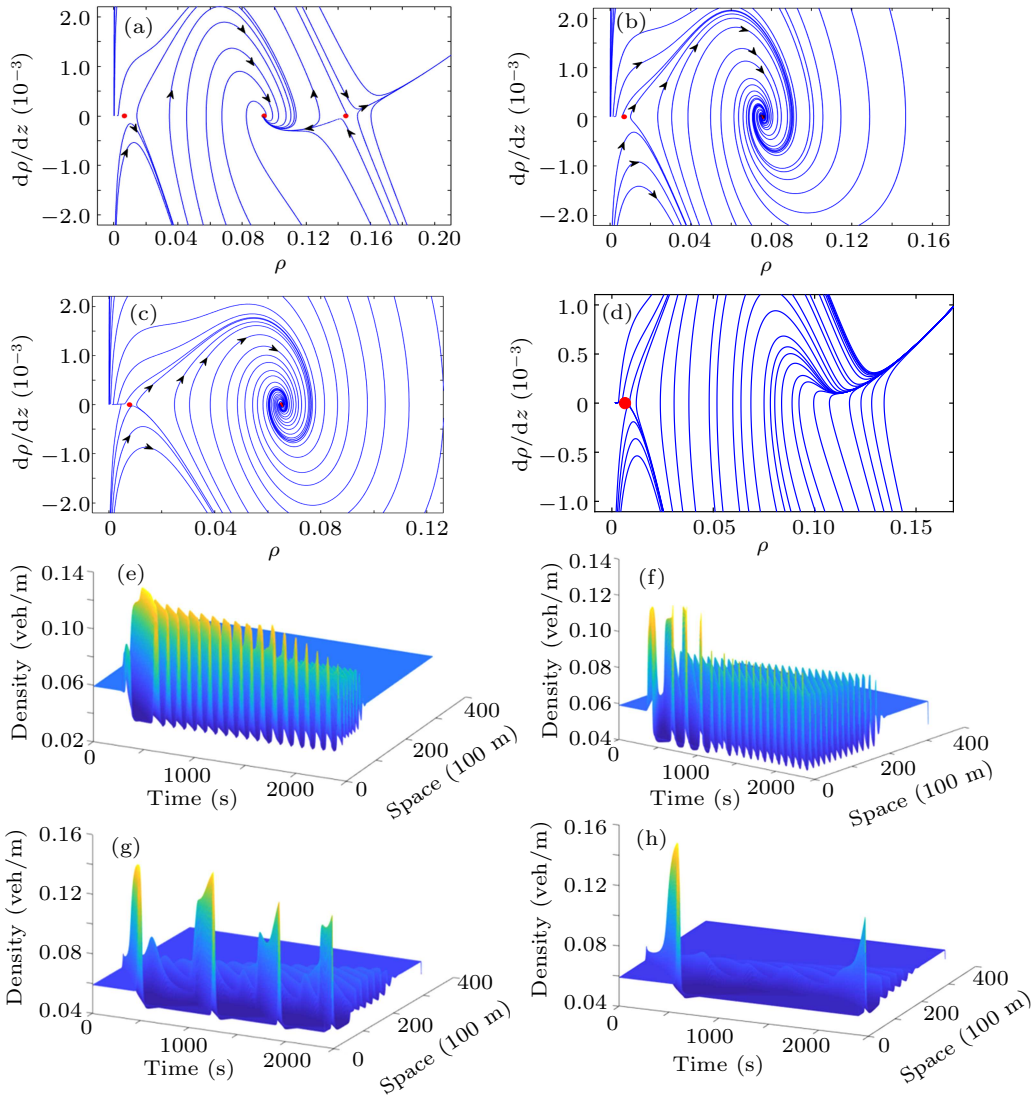


Fig. 8. System Hopf bifurcation variation phase plane diagrams for $k_1 = 0$ (a), 0.3 (b), 0.5 (c), and 0.8 (d), and density spatiotemporal diagrams for $k_1 = 0$ (e), 0.3 (b), 0.5 (c), and 0.8 (d), respectively.

When the system is added to the feedback control, it can be seen from Figs. 8(b)–8(d) that the system state changes differently when the control parameters take different values. The values of the parameters k_2 and k_3 are kept unchanged so as to study the effect of the control coefficient k_1 on the system. When $k_1 = 0.3$, the critical value of Hopf bifurcation of the controlled system will advance to $q_* = 0.787$. At this time, the system trajectory converges to the focal point $(0.078279, 0)$, and when $z \to +\infty$, the line trajectory in the figure converges to the focal point $(0.078279, 0)$, which indicates that the system state is stable at this equilibrium point, when $z \to -\infty$, the trajectory of the curve diverges to the far side and produces the oscillation phenomenon with the same amplitude, thus indicating that the system state at this point is unstable. Compared with Fig. 8(a), the Hopf bifurcation advancement occurs: when the parameter k_2 and k_3 are constant and $k_1 = 0.5$, the controlled system Hopf bifurcation critical value is advanced to $q_* = 0.826$. The corresponding system trajectory tends to be close to the equilibrium point $(0.065422, 0)$, when $z \to +\infty$, the trajectory tends to the focal

point $(0.065422, 0)$, indicating that the system state is stable at this equilibrium point; when $z \to -\infty$, the trajectory at the focal point diverges at a distant point and the system is unstable at this equilibrium point $(0.065422, 0)$. When $k_1 = 0.8$, $k_2 = 0.4$, and $k_3 = 0.6$, the Hopf bifurcation disappears at the equilibrium point $(0.089061, 0)$ as shown in Fig. 7(d).

From Fig. 8(e), it can be seen that when the system without control parameters passes through the Hopf bifurcation point, the amplitude of the initial small disturbance gradually increases with the spatiotemporal displacement, and a periodic oscillation phenomenon with equal amplitude appears in the system, reflecting the oscillation congestion phenomenon corresponding to the stop and go traffic. As the nonlinear feedback parameters of the system continue to increase, the state changes of the system are shown in Figs. 8(f)–8(h), indicating that the amplitude oscillation phenomenon changes with control parameters. When the parameters are controlled, as shown in Fig. 8(f), after adding small disturbances to the system, the oscillation amplitude of the system decreases with spatiotemporal displacement increasing. When the parameters are controlled as shown in Fig. 8(g), the phenomenon of constant amplitude oscillation in the system is significantly reduced. When the parameters are controlled, as shown in Fig. 8(h), the small disturbances added to the system dissipate over time and there is no fluctuation of time. At this point, the Hopf bifurcation of the system disappears and the traffic flow is in a smooth state.

Then the density spatiotemporal diagrams of the system before and after passing through the saddle junction bifurcation are plotted in Fig. 9 in order to analyze the state change of the system when it passes through this bifurcation point. In Fig. 9(a), the density spatiotemporal diagram before the system passes through the saddle junction bifurcation, and its initial density is 0.03 veh/m. From this diagram, it can be seen that when a small perturbation of amplitude 0.01 is added to the system, the perturbation dissipates with the spatiotemporal displacement and the system is in a stable state. Figure 9(b) shows the spatiotemporal plot of the density after passing through the saddle junction bifurcation point, with its initial density being 0.005 veh/m. It can also be seen from this figure that when a small perturbation is added to the system, the small perturbation in the system is amplified and the system becomes unstable, and the local clustering phenomenon observed in highway traffic occurs. From the changes of the system in Fig. 7, it can be concluded that the initial small perturbation disappears without any amplification because the value of the initial density is in a stable interval of the model. However, when the initial density value is greater than the density value of the saddle junction bifurcation point of the system, the system becomes unstable and the local clustering effect observed in freeway traffic appears as it evolves in time and space.

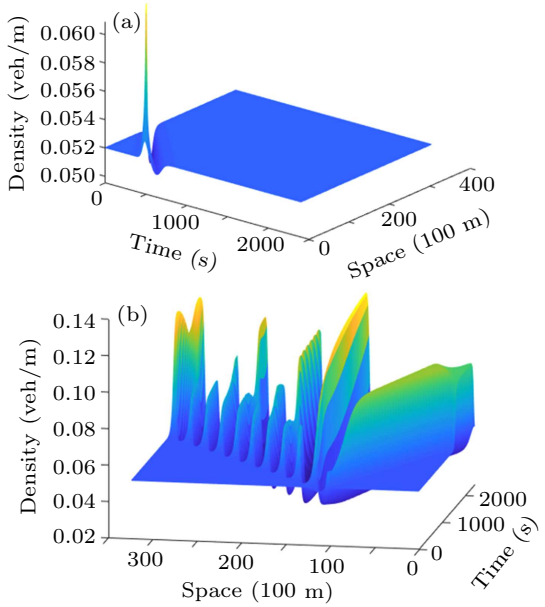


Fig. 9. Spatiotemporal plot of density of the system before and after passing through saddle junction bifurcation for $\rho_0 = 0.03$ veh/m (a) and 0.005 veh/m (b).

In Fig. 9(a), the traffic flow system is gradually stabilized before passing through the saddle junction bifurcation. The small perturbation on the initial density of the road section gradually decreases with time, indicating that the perturbation in the traffic flow disappears and tends to stabilize the process. The density of vehicles on the road section decreases, and the number of vehicles is reduced. The distance between cars is therefore larger, and the speed of vehicles is accelerated. The traffic flow will end up as a uniform traffic flow, and tends to be stable.

After the saddle junction bifurcation, in Fig. 9(b), the traffic flow system gradually tends to be unstable. The average density value of the road section gradually increases with the time fluctuation growing, which indicates that the disturbance in the traffic flow increases, the traffic loss is stabilized, and the complex local cluster structure appears. This situation corresponds to the stop-and-go phenomenon in the actual traffic. With the gradual increase of the vehicle density value, the number of vehicles on the road section increases, the inter-vehicle distance becomes smaller. Therefore the vehicle speed on the road section slows down, and the traffic flow system tends to be unstable.

In the following, we will conduct the simulation of the system density spatiotemporal maps by using the new model and the FVD model under the condition of the same initial density, respectively.

In Fig. 10, the following figure is divided into 2 sub-figures for ease of analysis: sub-figure 1 and sub-figure 2. The sub-figure 1 shows the density spatiotemporal map of the traditional FVD macro-model, including Figs. 10(a), 10(c), and 10(e). The sub-figure 2 displays the density spatiotemporal

map of the new model considering the connected car environment, including Figs. 10(b), 10(d), and 10(f): with Figs. 10(e) and 10(f) showing the density fluctuations of Figs. 10(c) and 10(d) at the same time.

It is found that under the same parameter conditions, small disturbances develop into single and multiple clusters as the initial density increases. Under the same initial density ρ, after the influence of vehicle networking factors is considered in the model, the traffic congestion can be effectively suppressed. Based on the simulation results of the FVD model and the new model considering the connected car factor, the following conclusions can be drawn: as can be seen from subfigures 1 and 2, with the increase of the initial density, the amplitude of the density wave amplifying from small perturbations to the appearance of near-periodic oscillatory-type oscillations is observed in both models.

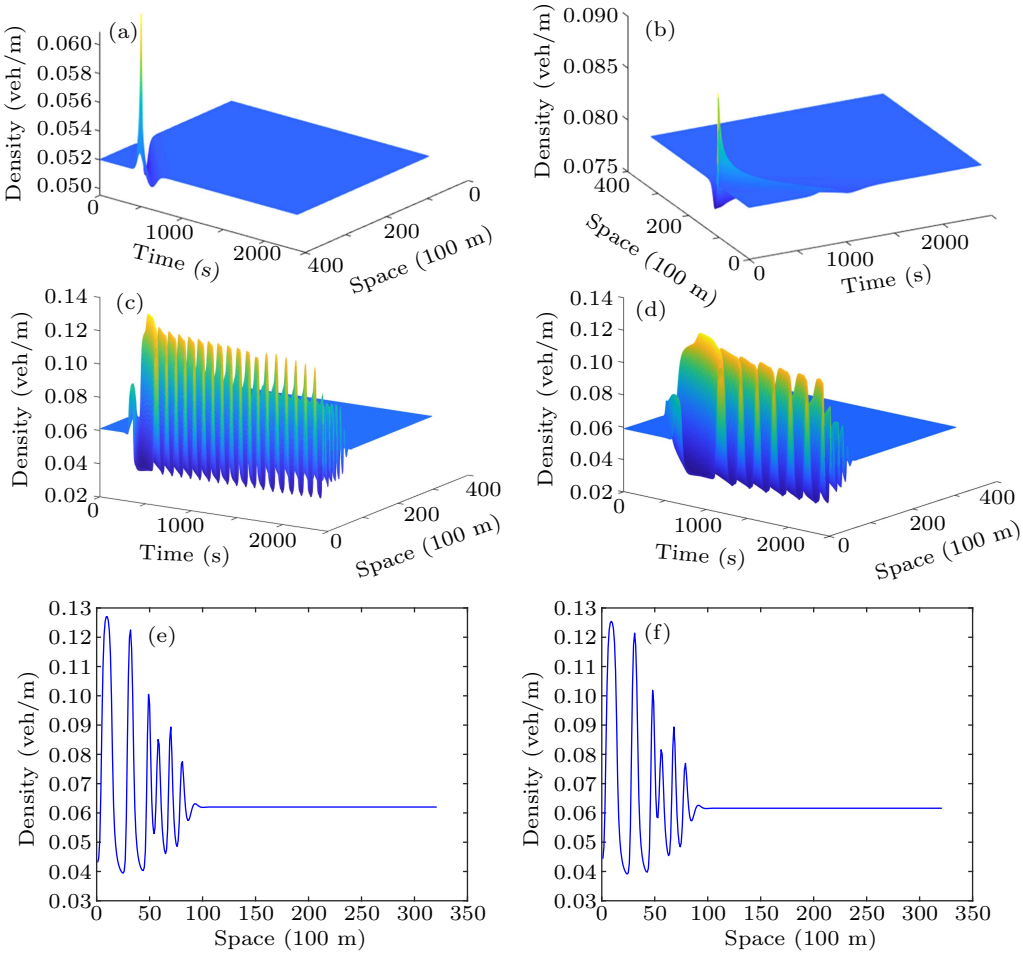


Fig. 10. Comparison of the FVD model with new model density spatiotemporal map simulations for different values of ρ_0: (a) $\rho_0 = 0.02$ veh/m (FVD model), (b) $\rho_0 = 0.02$ veh/m (new model), (c) $\rho_0 = 0.05$ veh/m (FVD model), (d) $\rho_0 = 0.05$ veh/m (new model), (e) $\rho_0 = 0.05$ veh/m (FVD model), (f) $\rho_0 = 0.05$ veh/m (new model).

However, comparing the density spatiotemporal plots of the FVD model on the left side and those of the new model on the right side (e.g., Fig. 10(c) versus Figs. 10(d) and 10(e) versus Fig. 10(f)), it can be found that the density oscillation of the FVD model is more intense under the same initial density condition, which indicates that the density fluctuation of traffic flow can be effectively reduced by adding the vehicle networking factor to the new model. In addition, compared with the FVD model, the new model has great traffic flow density when the system tends to stabilize. Therefore, the new model is more reasonable in terms of traffic stability.

Next, the density spatiotemporal maps of the traffic flow system for the new model and the GK model are plotted, respectively, under the same initial density conditions. It is shown as follows.

For ease of analysis, figure 11 is divided into two subfigures, i.e. sub-figure 1 and sub-figure 2. Sub-figure 1 includes the density spatiotemporal maps of the traditional GK model, as shown in Figs. 11(a), 11(c), and 11(e). Sub-figure 2, on the other hand, shows the density spatiotemporal maps of the new model that considers the connected car environment as described in Figs. 11(b), 11(d), and 11(f). Figures 11(e) and 11(f) show the simultaneous density fluctuations in Figs. 11(c) and 11(d).

It is found that under the same parameter conditions, small perturbations evolve into single or multiple density clus-

ters as the initial density increases. Under the same initial density, the introduction of vehicle networking factor in the new model can effectively suppress traffic congestion. By observing the simulation results of the GK model and the new model, the following conclusions are drawn: from sub-figures 1 and 2, it can be seen that with the increase of the initial density, both models show the phenomenon of the increase of amplitude of the density wave amplified from the small perturbations to the near-periodic oscillations.

By comparing the density spatiotemporal plots of the GK model on the left side with those of the new model on the right side (e.g., Fig. 11(c) versus Fig. 11(d) and Fig. 11(e) versus Fig. 11(f)), it can be observed that the density fluctuation of the GK model is very significant under the same initial density condition. This indicates that the density fluctuation of traffic flow can be effectively reduced after introducing the vehicle networking factor into the new model. In addition, compared with the GK model, the new model has a high density of traffic flow when the system tends to stabilize. Therefore, it can be concluded that the new model is more reasonable in terms of traffic stability. Next, we will compare the three models by using a tabular format.

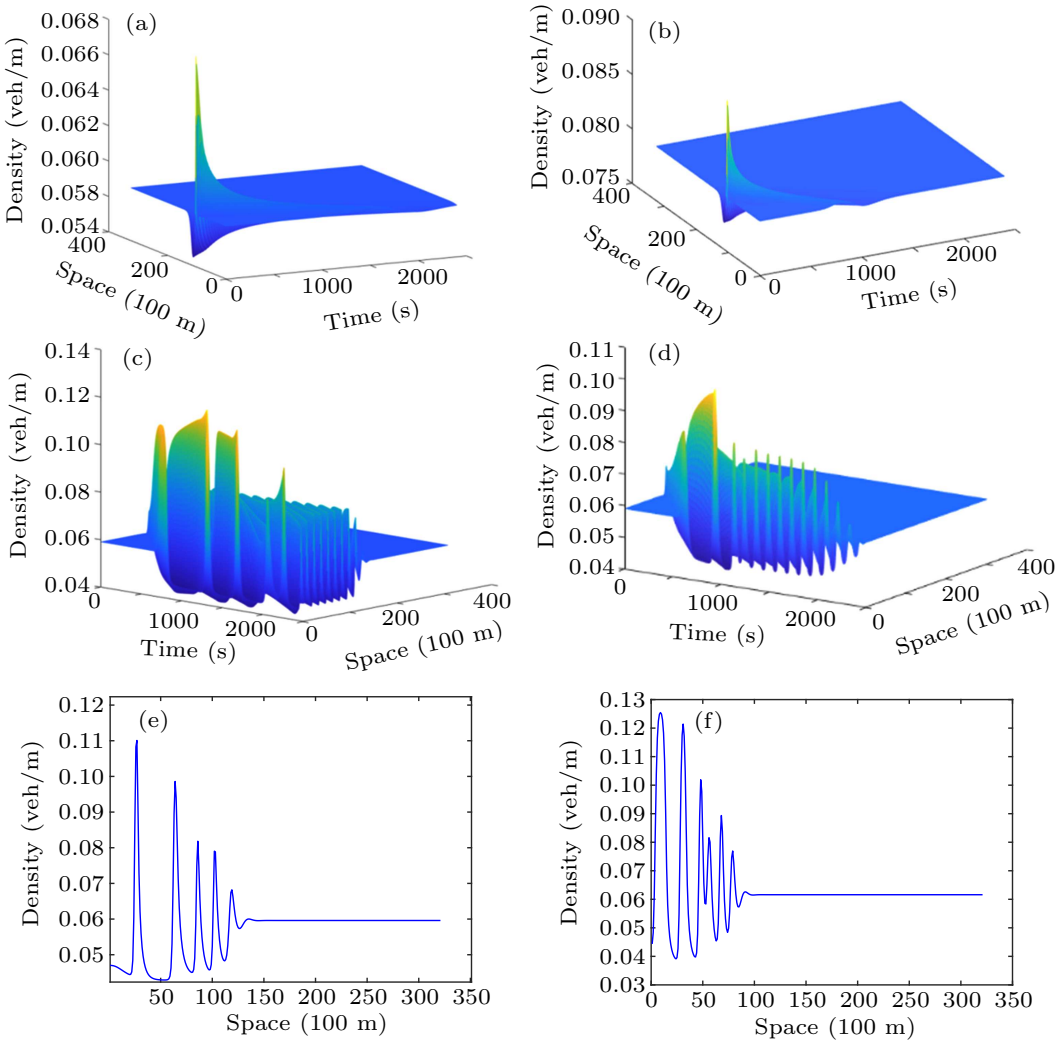


Fig. 11. Comparison of density spatiotemporal map simulations between GK model with new model: (a) $\rho_0 = 0.02$ veh/m (GK model), (b) $\rho_0 = 0.02$ veh/m (new model), (c) $\rho_0 = 0.05$ veh/m (GK model), (d) $\rho_0 = 0.05$ veh/m (new model), (e) $\rho_0 = 0.05$ veh/m (GK model), (f) $\rho_0 = 0.05$ veh/m (new model).

Table 3. Comparisons of traffic flow density data among three models.

Distance span (m)	Average density (veh/m)			Density fluctuation range (veh/m)		
	FVD	GK	CVM	FVD	GK	CVM
0–50	0.079	0.068	0.067	0.038–0.112	0–0.095	0.038–0.095
50–100	0.066	0.061	0.065	0.042–0.094	0–0.078	0.043–0.088
100–150	0.058	0.053	0.059	0.058–0.061	0.047–0.074	0.059–0.060
Average	0.067	0.060	0.063	–	–	–

From Table 3, it can be seen that for the average density values, there is not much difference among the three models on the same road section, with the maximum FVD being 0.067, the minimum GK being 0.060, and the CVM being 0.063 between the two. For the density fluctuation range indicator, the GK model has the highest density fluctuation among the three models, and even zero. The corresponding density fluctuation values of CVM are lower than those of the other two models, reflecting a relatively stable traffic flow. In terms of variance, the CVM model has a variance 29% lower than FVD and 58% lower than GK model. Therefore, it can be concluded that compared with FVD model and GK model, connected vehicle model (CVM) is very suitable for describing the traffic phenomenon of urban freeways under the vehicle networking factors considered in this work.

7. Conclusions

In this work, the integration of bifurcation control theory and traffic flow theory in nonlinear dynamics is discussed, with a focus on attempting to solve the problems such as the analysis and control of the stability suddenly changing behavior of traffic system. First, a new model is established by considering the influencing factors of adaptive cruise control system, and various bifurcation conditions of the system, such as Hopf bifurcation, saddle-knot bifurcation, BT bifurcation, etc., are derived through the combination of stability analysis and bifurcation analysis. Traffic phenomena such as time-walking and stability's sudden changes triggered by bifurcation points can be better explained by the density spatiotemporal map and phase plane map of the traffic system. In this work, a feedback controller is designed for the unstable bifurcation points of the traffic flow model to change the time of the bifurcation points occurring by adjusting the traffic flow parameters so that the unstable bifurcation points disappear. The effect of the feedback controller on Hopf bifurcation of traffic flow is investigated through numerical simulation, and the occurrence of Hopf bifurcation is delayed or eliminated by changing the control parameters of the feedback controller, which reduces the periodic oscillation phenomenon of the traffic density, and thus realizing the mitigation or preventive control of traffic congestion. In this work, new models and methods required for the prevention and control of sudden road changes in behavior are investigated, and the control strategies for unstable branching points such as saddle-knot bifurcation and BT bifurcation are designed for future work.

Appendix A: Deduction of conditions for existence of saddle node bifurcation

As mentioned earlier,

$$a=\boldsymbol{\psi}\cdot\frac{\partial}{\partial q_*}\boldsymbol{f}(\boldsymbol{x},q_*)\Big|_{(x_0,q_{*0})}=\begin{pmatrix}\dfrac{2}{(\lambda+M)\Delta^2}\left((\lambda+M)\Delta-\dfrac{q_{*0}}{\rho_0}\right) & 1\end{pmatrix}\begin{pmatrix}0\\ -\dfrac{2\rho_0}{T(\lambda+M)\Delta^2 q_{*0}}\end{pmatrix}=-\frac{2\rho_0}{T(\lambda+M)\Delta^2 q_{*0}}\neq 0, \tag{A1}$$

$$b=\boldsymbol{\psi}\cdot\sum_{i=1}^{n}e_i\left[\boldsymbol{\phi}^{\mathrm{T}}\frac{\partial^2}{\partial\boldsymbol{x}^2}\boldsymbol{f}_i(\boldsymbol{x},\lambda)\Big|_{(x_0,\lambda_0)}\boldsymbol{\phi}\right], \tag{A2}$$

where $\boldsymbol{\psi}=\begin{pmatrix}\dfrac{2}{(\lambda+M)\Delta^2}\left((\lambda+M)\Delta-\dfrac{q_{*0}}{\rho_0}\right) & 1\end{pmatrix}$, $\boldsymbol{\phi}=\begin{pmatrix}1\\0\end{pmatrix}$.

For system (11), let q_* be a variable parameter which has an equilibrium point $(\eta_0,0)$ for any value of q_*, then the derivative matrix at the equilibrium point will be

$$\boldsymbol{L}(q_*)=\begin{pmatrix}0 & 1\\ \dfrac{-2\rho_i}{T(\lambda+M)\Delta^2 q_*}[c-\rho_i V_{\mathrm{e}}'(\rho_i)-V_{\mathrm{e}}(\rho_i)] & \dfrac{2}{(\lambda+M)\Delta^2}(\dfrac{q_*}{\rho}-\lambda\Delta-M\Delta)\end{pmatrix}\Bigg|_{\substack{\rho=\rho_0\\ q^*=q_0^*}}\triangleq\begin{pmatrix}b_1 & b_2\\ b_3 & b_4\end{pmatrix}. \tag{A3}$$

Due to $\boldsymbol{L}=D_x\boldsymbol{f}(\boldsymbol{x},\lambda)\big|_{(x_0,\lambda_0)}$, then

$$\begin{aligned}\frac{\partial^2}{\partial\boldsymbol{x}^2}\boldsymbol{f}_i(\boldsymbol{x},\lambda)\big|_{(x_0,\lambda_0)}&=\frac{\partial}{\partial\rho}\boldsymbol{L}(q_*)=\frac{\partial}{\partial\rho}\left(\frac{-2\rho_i}{T(\lambda+M)\Delta^2 q_*}[c-\rho_i V_{\mathrm{e}}'(\rho_i)-V_{\mathrm{e}}(\rho_i)]\right)=\frac{-2\rho_i c+2\rho_i^2 V_{\mathrm{e}}'(\rho_i)+2\rho_i V_{\mathrm{e}}(\rho_i)}{T(\lambda+M)\Delta^2 q_*}\\ &=\frac{\dfrac{\partial}{\partial\rho}\left[-2\rho_i c+2\rho_i^2 V_{\mathrm{e}}'(\rho_i)+2\rho_i V_{\mathrm{e}}(\rho_i)\right]T(\lambda+M)\Delta^2 q_*-\dfrac{\partial}{\partial\rho}T(\lambda+M)\Delta^2 q_*\left[-2\rho_i c+2\rho_i^2 V_{\mathrm{e}}'(\rho_i)+2\rho_i V_{\mathrm{e}}(\rho_i)\right]}{\left(T(\lambda+M)\Delta^2 q_*\right)^2}\\ &=\frac{\left[-2c+4\rho_i V_{\mathrm{e}}'(\rho_i)+2\rho_i V_{\mathrm{e}}''(\rho_i)+2V_{\mathrm{e}}(\rho_i)+2\rho_i V_{\mathrm{e}}'(\rho_i)\right]T(\lambda+M)\Delta^2 q_*}{\left(T(\lambda+M)\Delta^2 q_*\right)^2}\\ &\quad-\frac{T(\lambda+M)\Delta^2 c\left[-2\rho_i c+2\rho_i^2 V_{\mathrm{e}}'(\rho_i)+2\rho_i V_{\mathrm{e}}(\rho_i)\right]}{\left(T(\lambda+M)\Delta^2 q_*\right)^2}.\end{aligned} \tag{A4}$$

Due to $q_* = -c\rho$, replacing $T(\lambda+M)\Delta^2 c\left[-2\rho_i c + 2\rho_i^2 V_e'(\rho_i) + 2\rho_i V_e(\rho_i)\right] = T(\lambda+M)\Delta^2 q_*\left[-2c + 2\rho_i V_e'(\rho_i) + 2V_e(\rho_i)\right]$ with Eq. (A4) yields

$$\begin{aligned}
&\frac{\partial^2}{\partial \boldsymbol{x}^2}\boldsymbol{f}_i(\boldsymbol{x},\lambda)\big|_{(x_0,\lambda_0)} \\
&= \frac{\left[-2c + 4\rho_i V_e'(\rho_i) + 2\rho_i V_e''(\rho_i) + 2V_e(\rho_i) + 2\rho_i V_e'(\rho_i)\right] T(\lambda+M)\Delta^2 q_*}{\left(T(\lambda+M)\Delta^2 q_*\right)^2} - \frac{T(\lambda+M)\Delta^2 q_*\left[2c - 2\rho_i V_e'(\rho_i) - 2V_e(\rho_i)\right]}{\left(T(\lambda+M)\Delta^2 q_*\right)^2} \\
&= \frac{\left[-2c + 4\rho_i V_e'(\rho_i) + 2\rho_i V_e''(\rho_i) + 2V_e(\rho_i) + 2\rho_i V_e'(\rho_i) - \left(2c - 2\rho_i V_e'(\rho_i) - 2V_e(\rho_i)\right)\right] T(\lambda+M)\Delta^2 q_*}{\left(T(\lambda+M)\Delta^2 q_*\right)^2} \\
&= \frac{\left(4V_e(\rho_0) + 8\rho_0 V_e'(\rho_0) + 2\rho_0^2 V_e''(\rho_0) - 4c\right)\left(T(\lambda+M)\Delta^2 q_{*0}\right)}{\left(T(\lambda+M)\Delta^2 q_*\right)^2} = \frac{\left(4V_e(\rho_0) + 8\rho_0 V_e'(\rho_0) + 2\rho_0^2 V_e''(\rho_0) - 4c\right)}{\left(T(\lambda+M)\Delta^2 q_*\right)}.
\end{aligned} \tag{A5}$$

Replacing (A5) with $b = \psi \cdot \sum_{i=1}^{n} e_i[\phi^{\mathrm{T}} \frac{\partial^2}{\partial \boldsymbol{x}^2}\boldsymbol{f}_i(\boldsymbol{x},\lambda)\big|_{(x_0,\lambda_0)}\ \phi]$ leads to

$$\begin{aligned}
b &= \psi \cdot \sum_{i=1}^{n} e_i\left[\phi^{\mathrm{T}} \frac{\partial^2}{\partial \boldsymbol{x}^2}\boldsymbol{f}_i(\boldsymbol{x},\lambda)\big|_{(x_0,\lambda_0)}\ \phi\right] \\
&= \begin{pmatrix} \dfrac{2}{(\lambda+M)\Delta^2}\left((\lambda+M)\Delta - \dfrac{q_{*0}}{\rho_0}\right) & 1 \end{pmatrix} \cdot \begin{pmatrix} (1\ 0)\begin{pmatrix} 0 & 0 \\ 0 & 0 \end{pmatrix}\begin{pmatrix} 1 \\ 0 \end{pmatrix} \\ (1\ 0)\begin{pmatrix} \dfrac{4V_e(\rho_0) + 8\rho_0 V_e'(\rho_0) + 2\rho_0^2 V_e''(\rho_0) - 4c}{T(\lambda+M)\Delta^2 q_{*0}} & -\dfrac{2q_*}{(\lambda+M)\Delta^2\rho_0^2} \\ -\dfrac{2q_*}{(\lambda+M)\Delta^2\rho_0^2} & 0 \end{pmatrix}\begin{pmatrix} 1 \\ 0 \end{pmatrix} \end{pmatrix} \\
&= \begin{pmatrix} \dfrac{2}{(\lambda+M)\Delta^2}\left((\lambda+M)\Delta - \dfrac{q_{*0}}{\rho_0}\right) & 1 \end{pmatrix} \cdot \begin{pmatrix} 0 \\ \left(\dfrac{4V_e(\rho_0) + 8\rho_0 V_e'(\rho_0) + 2\rho_0^2 V_e''(\rho_0) - 4c}{T(\lambda+M)\Delta^2 q_{*0}} \quad -\dfrac{2q_*}{(\lambda+M)\Delta^2\rho_0^2}\right)\begin{pmatrix} 1 \\ 0 \end{pmatrix} \end{pmatrix} \\
&= \begin{pmatrix} \dfrac{2}{(\lambda+M)\Delta^2}\left((\lambda+M)\Delta - \dfrac{q_{*0}}{\rho_0}\right) & 1 \end{pmatrix} \cdot \begin{pmatrix} 0 \\ \dfrac{4V_e(\rho_0) + 8\rho_0 V_e'(\rho_0) + 2\rho_0^2 V_e''(\rho_0) - 4c}{T(\lambda+M)\Delta^2 q_{*0}} \end{pmatrix} \\
&= \frac{4V_e(\rho_0) + 8\rho_0 V_e'(\rho_0) + 2\rho_0^2 V_e''(\rho_0) - 4c}{T(\lambda+M)\Delta^2 q_{*0}} \neq 0.
\end{aligned}$$

Acknowledgements

Project supported by the National Natural Science Foundation of China (Grant No. 72361031) and the Gansu Province University Youth Doctoral Support Project (Grant No. 2023QB-049).

References

[1] Wang Y, Tu H Z, Sze N N, Li H and Ruan X 2022 *J. Saf. Res.* **80** 1
[2] Ge H X, Dai S Q, Dong L Y and Xue Y 2004 *Phys. Rev. E* **70** 066134
[3] Gong Y and Zhu W X 2022 *Chin. Phys. B* **31** 024502
[4] Zhang Y F, Chen X H, Wang J P, Zheng Z D and Wu K 2022 *Transport. Res. C* **145** 103926
[5] Li X, Xiao Y W, Zhao X D, Ma X Wang and Wang X T 2023 *Physica A* **609** 128368
[6] Cheng R J, Ge H X and Wang J F 2018 *Appl. Math. Comput.* **332** 493
[7] Wang X N, Liu M Z, Ci Y S and Wu L N 2022 *Physica A* **607** 128196
[8] Jin Y F and Xu M 2010 *Chin. Phys. Lett.* **27** 040501
[9] Qin S D, Cheng R J and Ge H X 2018 *Chin. Phys. B* **27** 050503
[10] Zhang Q L and Liu S Z 2023 *Appl. Math. Comput.* **436** 127502
[11] Mohamed K and Abdelrahman M A E 2023 *Appl. Math. Comput.* **42** 53
[12] Zhao H X, Zhan J Y and Zhang L G 2023 *Syst. Control. Lett.* **173** 105465
[13] Wen J H, Hong L J, Dai M, Xiao X P and Wu C Z 2023 *Appl. Math. Comput.* **440** 127637
[14] Zhang Y C, Xue Y, Zhang P, Fan D L and He H D 2019 *Physica A* **514** 133
[15] Ngoduy D and Li T 2020 *Transport. A* **17** 878
[16] Jin Y F and Meng J W 2020 *Commun. Nonlinear Sci. Numer. Simul.* **90** 105333
[17] Petersik P, Panja D and Dijkstra H A 2021 *Physica D* **427** 133016
[18] Li T 2005 *Physica D* **207** 41
[19] Sun Y Q, Ge H X and Cheng R J 2019 *Physica A* **521** 752
[20] Ren W L, Cheng R J and Ge H X 2021 *Appl. Math. Comput.* **401** 126079
[21] Ren W L, Cheng R J and Ge H X 2021 *Appl. Math. Model.* **94** 369
[22] Lyu H, Cheng R J and Ge H X 2022 *Physica A* **585** 126434
[23] Kaur R and Sharma S 2018 *Physica A* **510** 446
[24] Jiang R, Wu Q and Zhu Z 2001 *Phys. Rev. E* **64** 017101
[25] Zhai C and Wu W 2021 *Commun. Nonlinear Sci. Numer. Simul.* **95** 105667
[26] Jiang C T, Ge H X and Cheng R J 2019 *Physica A* **513** 465
[27] Hong K S 2012 *Phys. Lett. A* **376** 442
[28] Zhang Y C, Xue Y, Zhang P, Fan D L and He H D 2019 *Physica A* **514** 133
[29] Singh A and Sharma V S 2023 *J. Comput. Appl. Math.* **418** 114666
[30] Huang C D, Li H, Li T X and Chen S J 2019 *Int. J. Bifurc. Chaos.* **29** 1950150
[31] Zhai Q T, Ge H X and Cheng R J 2018 *Physica A* **490** 774

[32] Redhu P and Gupta A K 2015 *Commun. Nonlinear Sci. Numer. Simul.* **27** 263
[33] Cheng L F, Wei X K and Cao H J 2018 *Nonlinear Dyn.* **93** 42415
[34] Wang Y Q, Yan B W, Zhou C F, Li W K and Jia B 2018 *Mod. Phys. Lett. B* **32** 1850118
[35] Kamath G K, Jagannathan K and Raina G 2019 *Nonlinear Dyn.* **96** 185
[36] Newell G F 1961 *Operations Res.* **9** 209
[37] Ren W L, Cheng R J and Ge H X 2021 *Appl. Math. Model.* **94** 369
[38] Guan X Y, Cheng R J and Ge H X 2021 *Physica A* **574** 125972
[39] Yang Q L 2023 *Appl. Math. Model.* **116** 415
[40] Gazis D C and Rothery H R W 1961 *Operations Res.* **9** 545
[41] Herman R, Montroll E W, Potts R B and Rothery R W 1959 *Operations Res.* **7** 86
[42] Ai W H, Zhu J N, Zhang Y F, Wang M M and Liu D W 2023 *Physica A* **624** 128961